ACS OMEGA

Open Access

http://pubs.acs.org/journal/acsodf

Article

Identification of Novel Quinolone and Quinazoline Alkaloids as Phosphodiesterase 10A Inhibitors for Parkinson's Disease through a Computational Approach

Iqra Ahmad, Hira Khalid, Asia Perveen, Muhammad Shehroz, Umar Nishan, Faiz Ur Rahman, Sheheryar, Arlindo Alencar Moura, Riaz Ullah, Essam A. Ali, Mohibullah Shah,* and Suvash Chandra Ojha*

Cite This: *ACS Omega* 2024, 9, 16262−16278

Read Online

ACCESS | Metrics & More | Article Recommendations | Supporting Information

ABSTRACT: Phosphodiesterases (PDEs) are vital in signal transduction, specifically by hydrolyzing cAMP and cGMP. Within the PDE family, PDE10A is notable for its prominence in the striatum and its regulatory function over neurotransmitters in medium-spiny neurons. Given the dopamine deficiency in Parkinson's disease (PD) that affects striatal pathways, PDE10A inhibitors could offer therapeutic benefits by modulating D1 and D2 receptor signaling. This study was motivated by the successful history of quinazoline/quinazoline scaffolds in the inhibition of PDE10A. This study involved detailed *in silico* evaluations through docking followed by pharmacological, pharmacophoric, and pharmacokinetic analyses, prioritizing central nervous system (CNS)-active drug criteria. Seven cyclic peptides, those featuring the quinazoline/quinazoline moiety at both termini, exhibited notably enhanced docking scores compared to those of the remaining alkaloids within the screened library. We identified 7 quinolines and 1 quinazoline including Lepadin G, Aspernigerin, CJ-13536, Aurachin A, 2-Undecyl-4(1*H*)-quinolone, Huajiaosimuline 3-Prenyl-4-prenyloxyquinolin-2-one, and Isaindigotone that followed the standard CNS active drug criteria. The dominant quinoline ring in our study and its related quinazoline were central to our evaluations; therefore, the pharmacophoric features of these scaffolds were highlighted. The top alkaloids met all CNS-active drug properties; while nonmutagenic and without PAINS alerts, many indicated potential hepatotoxicity. Among the compounds, Huajiaosimuline was particularly significant due to its alignment with lead-likeness and CNS-active criteria. Aspernigerin demonstrated its affinity for numerous dopamine receptors, which signifies its potential to alter dopaminergic neurotransmission that is directly related to PD. Interestingly, the majority of these alkaloids had biological targets primarily associated with G protein-coupled receptors, critical in PD pathophysiology. They exhibit superior excretion parameters and toxicity end-points compared to the standard. Notably, selected alkaloids demonstrated stability in the binding pocket of PDE10A according to the molecular dynamic simulation results. Our findings emphasize the potential of these alkaloids as PDE10A inhibitors. Further experimental studies may be necessary to confirm their actual potency in inhibiting PDE10A before exploring their therapeutic potential in PD.

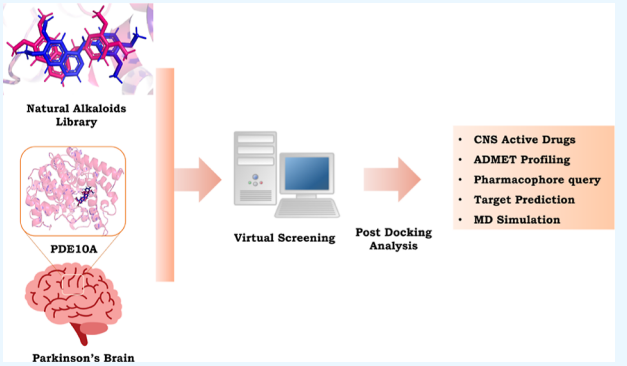

1. INTRODUCTION

Phosphodiesterases (PDEs) hydrolyze cyclic adenosine monophosphate (cAMP) and cyclic guanosine monophosphate (cGMP). It is involved in the regulation of signal transduction pathways mediated by these secondary messengers. Inactivated 5′-AMP and 5′-GMP are formed by the hydrolases of active cAMP and cGMP, respectively.[1] The brain, especially the striatum, has many PDEs, as shown by the presence of mRNA and protein. Studies with PDE knockout mice highlight its role in striatal dopaminergic neurons and the potential of PDE inhibitors for treating central nervous system (CNS) disorders.[2,3]

PDE10A, abundant in the striatum, regulates many neurotransmitters in medium-spine neurons (medium-spiny neurons). Its role in striatal signaling makes it a study target for neurodegenerative disorders like schizophrenia and Huntington's disease,[3,4] and it is also being explored for Parkinson's disease (PD) treatment.[5] PD is the second most common neurodegenerative disorder after Alzheimer's disease and is characterized by a deficiency of dopamine, which causes inhibition of the striatonigral and activation of the striatopallidal pathways. The imbalance of these two efferent

Received: December 25, 2023
Revised: March 12, 2024
Accepted: March 13, 2024
Published: March 26, 2024

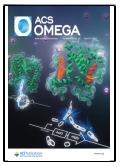

pathways in the striatum leads to the overstimulation of GABAergic neurons from the basal ganglia to the thalamus.[6] However, L-DOPA (L-3,4-dihydroxyphenylalanine), a precursor of dopamine, is still a standard treatment for PD; however, the appearance of side effects like dyskinesias and on−off phenomena has reduced its efficacy.[7] Consequently, there is a need for new drugs that can mitigate L-DOPA side effects along with treating PD.

PDE10A inhibitors increase D1 receptor signaling and decrease D2 receptor signaling; hence, the functioning of both striatonigral and striatopallidal outputs is regulated, respectively.[8] Also, it causes the activation of immediate early genes, an increase in the expression of proenkephalin in striatopallidal neurons, and an increase in the expression of preprotachykinin in striatonigral neurons.[9] The role of PDE10A in striatal signaling highlights its potential as a therapeutic target for PD.

A quinazoline alkaloid and analogue of isoquinoline, papaverine was first used as a PDE10A inhibitor to demonstrate its antipsychotic activity.[10,11] Papaverine increased cAMP and cGMP in the mouse striatum in the conditioned avoidance model, an effect reduced in PDE10A knockout mice, suggesting PDE10A inhibition by papaverine.[11] Additionally, papaverine showed positive effects in various behavioral models.[12] These roles of papaverine led to its use as a reference in a number of studies aiming to design and optimize new leads for PDE10A inhibition.[13] But the lack of selectivity of papaverine on other PDE isoforms has remained a problem in many studies, and due to this reason, papaverine is regarded as a nonselective PDE10A inhibitor.[13]

The association between PDE10A and quinoline- and quinazoline-based inhibitors is well recognized in the biochemical field. Numerous studies have explored the potential of these types of inhibitors for PDE10A. As mentioned before, quinazoline/isoquinoline papaverine was the first potent inhibitor of PDE10A, which was reported in 2006 by Siuciak et al.[11] This discovery was followed by a patent by Pfizer in the same year (2006), in which they reported dimethoxyquinazoline as a potent PDE10A inhibitor related to papaverine.[14] Later, in 2011, Kehler et al. described the highly efficient binding of novel triazoloquinazolines with PDE10A.[15] It was followed shortly by pyrazoloquinoline analogues, which were found to bind with PDE10A and were reported to have PDE10A-inhibitory potential with high binding affinity.[16] Moreover, in 2012, Ho et al. reported the identification of potent and orally active dihydroimidazoisoquinolines as PDE10A inhibitors.[17] The SAR development of dihydroimidazoisoquinoline derivatives was studied by Ho et al. in 2012. This study claimed the hydrophobic interaction of the phenyl of dihydroisoquinoline with the Phe719 and Phe686 residues of PDE10A and reported the discovery of a dihydroimidazoisoquinoline derivative as a potent, selective, and orally active PDE10A inhibitor.[18] In 2014, Allergan patented substituted 6,7-dialkoxy-3-isoquinoline derivatives as PDE10A inhibitors.[19] Recently, in 2017, AbbiVie claimed the bicyclic derivatives as pharmaceutically suitable PDE10A inhibitors that were based on pyridazin-4-one, quinoline, and N-oxides[20]

Keeping in view the importance of this class of compounds, this study selected 238 alkaloids with quinoline and quinazoline scaffolds as an in-house library against the PDE10A receptor. Moreover, there is no commercial drug available with this scaffold other than papaverine, which is a nonselective PDE10A inhibitor. Selected 192 quinoline and 46 quinazoline alkaloids have been previously reported for a broad range of bioactivities, including antibacterial, antimalarial, and antitumor activities. The research will involve molecular docking to determine binding affinities and interactions with PDE10A, along with pharmacokinetics, ADMET profiling, and target prediction to assess the drug-likeness, safety parameters, and off-target effects of selected alkaloids. Molecular dynamics (MD) simulations will be conducted to evaluate the stability and behavior of protein−ligand complexes. The ultimate goal is to discover novel quinoline and quinazoline alkaloids, contributing to the development of more effective and safer treatments for PD.

2. MATERIALS AND METHODS

2.1. Retrieval of 3D Structures of Receptor Proteins. The three-dimensional (3D) structure of PDE10 with PDB code 6MSA and resolution 2.06 Å was downloaded as a receptor protein. This protein structure was selected based on high resolution, completeness of the side chain and active site, and the presence of a cocrystallized ligand in the active site.[21] Generally, protein structures with resolutions between 1.5 and 2.5 Å are strong candidates for further research.[22]

2.2. Refinement of Receptor Proteins. The protein structure of PDE10A was refined using molecular operating environment (MOE) software before docking studies.[23] Nonessential ligands and water molecules were removed for the preparation and enhancement of PDE10A. Hydrogen coordinate data are missing in most of the protein crystal structures due to the limited resolution, and they can affect ligand−protein interactions. Proper bond orders were assigned to the 3D structure of PDE10A by using default parameters. The energy (kcal/mol) of the target protein was minimized by the MOE using the MMFF94x force field with the conjugant gradient method. The protein file was saved in mdb format as an input file in the downstream study.

2.3. Determination of the Active Site of the Protein. Active site determination is pertinent to the interaction of proteins and ligands. The pdb file PDE10A was imported to the MOE, where the accessible pockets of the PDE10A were predicted by the "MOE-Site Finder Tool". Moreover, dummy atoms were generated at the docking target atoms to select the active site residues of the binding site. The docking positions are represented by these dummy atoms. Furthermore, for visualization, "alpha spheres" and "atoms and backbone" were selected at the render and isolate settings, respectively.

2.4. Ligand Database Preparation. The 2D structures of the biologically active quinoline and quinazoline alkaloids and the standard, papaverine, were drawn in ChemDraw 12.0 by using the simplified molecular-input line-entry system (SMILES) and saved in mol format. A database was prepared in which all of the ligands were converted into their 3D structures and used as input for MOE-docking. All the ligands were stabilized by energy minimization and further processed by using the default parameters, as reported previously.[23]

2.5. Molecular Docking. Molecular docking has become a crucial tool for predicting the binding affinity of a protein−ligand complex. The goal of docking studies is to determine the best-docked conformation of the hits and to investigate the critical interactions between the inhibitor and the target protein while the ligand is considered flexible and the protein is considered rigid.[24] The ligand database of quinoline and quinazoline alkaloids was docked into the active site of PDE10A by using MOE-Dock. Five conformations of each

https://doi.org/10.1021/acsomega.3c10351
ACS Omega 2024, 9, 16262−16278

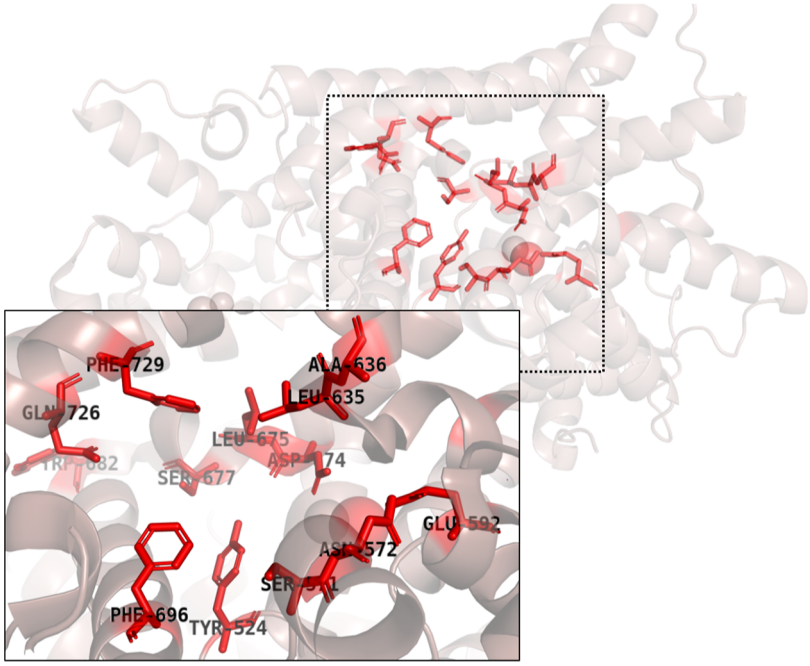

Figure 1. Active site residues (red) of receptor Phosphodiesterase 10A (PDE10A).

protein−ligand complex were generated, and the best conformations were checked by their binding free energies (S-score, kcal/mol) and analyzed by their binding interactions. The standard (papaverine) was also docked with the PDE10A by MOE-Dock at the active site predicted by the MOE-site finder tool. The docking score (S) of the standard was compared with the score of all of the interacted alkaloids. All the protein−ligand complexes that showed a higher S-score than those of the standards were selected for postdocking studies. In order to exclude the false-positive results and check the reliability of our prediction method, a Camptothecin derivative, namely, Irinotecan (CPT-11), approved as a drug for cancer treatment, was also docked with PDE10A.

2.6. Validation of Docking Protocol. To ensure the accuracy and reliability of the screening through docking, we used a systematic validation process that included redocking and superimposition methods.[23,25] The reference alkaloid, papaverine, was docked into the specified active site of the PDE10A (PDB ID: 6MSA) using the MOE software. The resulting lowest energy pose of the papaverine−PDE10A complex was analyzed, and the characteristics of the ligand−protein binding site were recorded. Afterward, papaverine was separated from the papaverine−PDE10A complex and redocked, maintaining the same binding parameters. The final lowest energy poses of both the docked and redocked complexes were superimposed in PyMOL to determine the executive root-mean-square deviation (rmsd) value. An rmsd value of ≤2 Å or 0.2 nm is typically accepted as confirmation of a reliable docking method.[26]

2.7. Generation of Essential Pharmacophores. After a thorough examination of ligand interactions among the most prominent alkaloids, a unique interaction with the sulfur atom was discovered. As a result, all significant interactions were annotated using a single structure, leading to the creation of an extensive pharmacophore.[27] A high-quality pharmacophore model was developed with Pharmacaphore Query Editor in MOE, which can generate a variety of predefined pharmacophore features, such as hydrogen bond donor (Don), hydrogen bond acceptor (Acc), aromatic center (Aro), Pi ring center (PiR), aromatic ring or Pi ring normal (PiN), hydrophobic (Hyd), anionic atom (Ani), and cationic atom (Cat), among others. The radius of the detected pharmacophore features was calibrated to 1.0 Å, and the distances between the features were measured.

2.8. Pharmacokinetics and ADMET Analysis. Swiss ADME (www.swissadme.ch) software of the Swiss Institute of Bioinformatics (http://www.sib.swiss) and PkCSM (https://biosig.lab.uq.edu.au/pkcsm) were employed to estimate the blood−brain barrier (BBB) permeability and individual ADME behaviors expressed on the basis of Lipinski's Rule of CNS-active drug criterion.[28] Additionally, ADMETlab 2.0 (https://admetmesh.scbdd.com/) and ProTox-II (https://tox-new.charite.de) were employed to predict excretion and toxicity end-point parameters, respectively. The list was made to contain one input per molecule, formatted as a SMILES, and the results were downloaded for each molecule in an Excel spreadsheet. These tools were also accessed for the analysis of the CNS activity, drug−drug interactions, toxicity, and medicinal chemistry of the top alkaloids.

2.9. Swiss Target Prediction. The top alkaloids were subjected to Swiss target prediction analysis. It was used to find potential biological targets, in addition to their predicted affinity for PDE10A. It is a tool that predicts the potential protein targets of a small molecule. The output is given in terms of possible targets ranked by probability. For this study, we concentrated specifically on the features of the top 15 predicted targets of the selected alkaloids. We related them to the pathophysiology of PD to emphasize the fundamental goal of identifying the possible neuroprotective activities of our alkaloids.

2.10. Molecular Dynamics Simulations. MD simulations were executed to investigate the dynamic interactions between the three selected alkaloids and the protein PDE10A. Schrödinger LLC Desmond software[29] was employed for these simulations, which spanned a duration of 30 ns for each alkaloid−protein complex. Utilizing Newton's classical motion

https://doi.org/10.1021/acsomega.3c10351
ACS Omega 2024, 9, 16262−16278

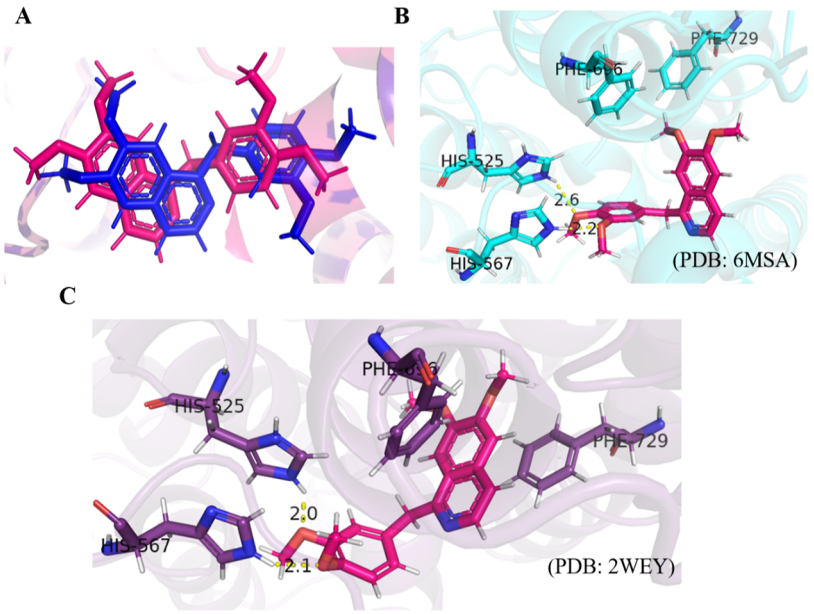

Figure 2. (A) Superimposition of docked (blue) and reference or redocked (pink) papaverine−PDE10A complexes. (B) interactions between papaverine and PDE10A (PDB: 6MSA). (C) interactions between papaverine and PDE10A (PDB: 2WEY).

equations, the simulations provided a detailed understanding of the dynamic behavior of the alkaloids by monitoring the movements of individual atoms within the complexes. To prepare the alkaloid−PDE10A complexes for the simulations, Schrödinger's Maestro was employed.[30] This preparation involved optimization processes, minimization, and the addition of any missing residues to ensure the integrity of the system. The solvent environment for the simulations was modeled using a 3-point transferable solvent model. It was housed within an orthorhombic simulation box with the OPLS_2005 force field.[31]

The simulations were conducted under specific conditions, maintaining a temperature of 300 K and a pressure of 1 atm. To replicate physiological conditions and ensure the neutrality of the models, counterions were introduced along with a sodium chloride concentration of 0.15 M. Prior to the commencement of the simulations, each model underwent a relaxation phase during which the constraints on the system were progressively released. The trajectories of these simulations were meticulously recorded for subsequent analysis. The stability and behavior of the alkaloid−PDE10A complexes were further assessed. For this, root-mean-square fluctuation (rmsf) and rmsd plots were used.

3. RESULTS AND DISCUSSION

3.1. Active Site Prediction. The MOE-site finder tool predicted the active site based on manually applied settings. Active sites of the receptor protein were predicted on the basis of the cocrystallized ligand and confirmed through the literature.[32,33] Residues in the active site included Tyr524, Ser571, Asn572, Glu592, Leu635, Ala636, Asp674, Leu675, Ser677, Ile692, Phe696, Gln726, and Phe729. The binding sites of PDE10A are composed of a core pocket that contains an invariant substrate-recognizing Gln726 residue, which is critical for substrate or ligand recognition. Also, the binding site contains conserved aromatic Phe729, located at the roof of the hydrophobic clamp (P-clamp), and two hydrophobic residues, Ile629 and Phe696, in PDE10A, located on the floor of the binding site. Hence, the crucial interactions responsible for inhibiting PDE10A activities involve a hydrophobic interaction with the residues that form the P-clamp.[34] Therefore, the residues of particular importance are Ile629, Phe696, and Gln726[34] (Figure 1).

3.2. Docking Protocol Verification. In molecular docking, the precise location of the ligand within the target protein structure is a prerequisite. One important metric for assessing this accuracy is the rmsd,[23] which measures the average distance between atoms in superimposed complexes and indicates the degree of similarity between the docked and redocked structures. An rmsd value that is closer to zero indicates that the docked pose closely resembles the reference structure, indicating the reliability of the docking process.

In the superimposition analysis of the docked and redocked papaverine−PDE10A complexes, there was an initial comparison between 328 atoms of each by pairwise scoring. During the refinement process, a series of alignment cycles were done that did not reject any atoms, resulting in a final alignment between all 328 atoms in each structure. The executive rmsd value obtained was 0.00 Å, indicating almost identical alignment between the docked and redocked structures without any deviations (Figure 2A,B). Collectively, these results emphasize the precision of the docking methodologies as the docked standard alkaloids closely align with their respective complexes. We may conclude that the same technique will probably provide accurate poses for the studied alkaloids in the library received from the curated literature survey. It shows that our docking protocol can reproduce the known poses of reference compounds with the described precision.

3.3. Protein−Ligand Interactions. The interacting alkaloids were sorted according to their binding energies using the docking scoring of the MOE software. Papaverine was used as a standard alkaloid for the PDE10A receptor. An in-house library consists of quinoline (192) and quinazoline (47) alkaloids that were subjected to docking against PDE10A, and papaverine was used as a standard. In this process, 2

https://doi.org/10.1021/acsomega.3c10351
ACS Omega 2024, 9, 16262−16278

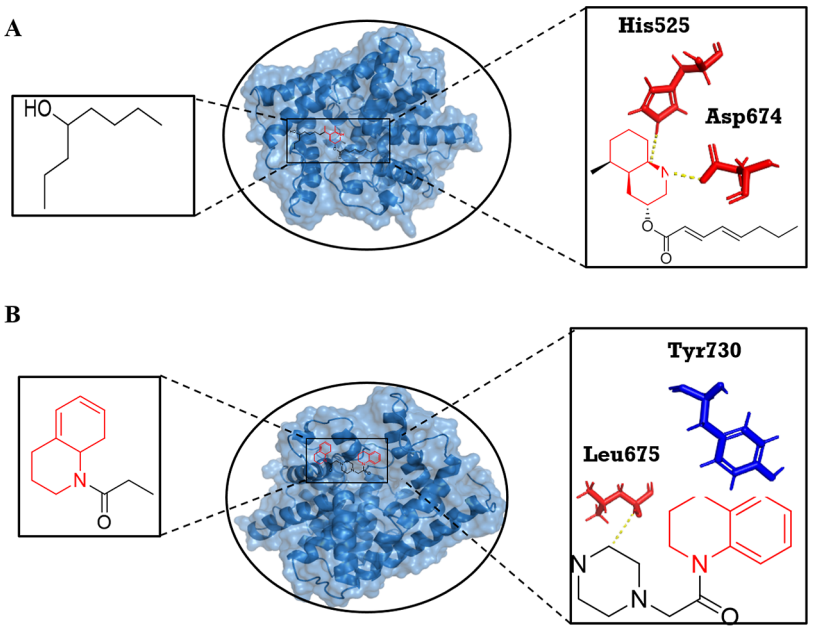

Figure 3. Molecular interactions of Lepadin G (A) and Aspernigerin (B) with PDE10A, with a focus on the major quinoline structure (at right), highlighted in red, and the remaining portion (at left), featuring their respective interactions with PDE10A. Red-colored residues are bonded by H-bonding, and blue-colored residues are bonded with pi−pi or H−pi bonding.

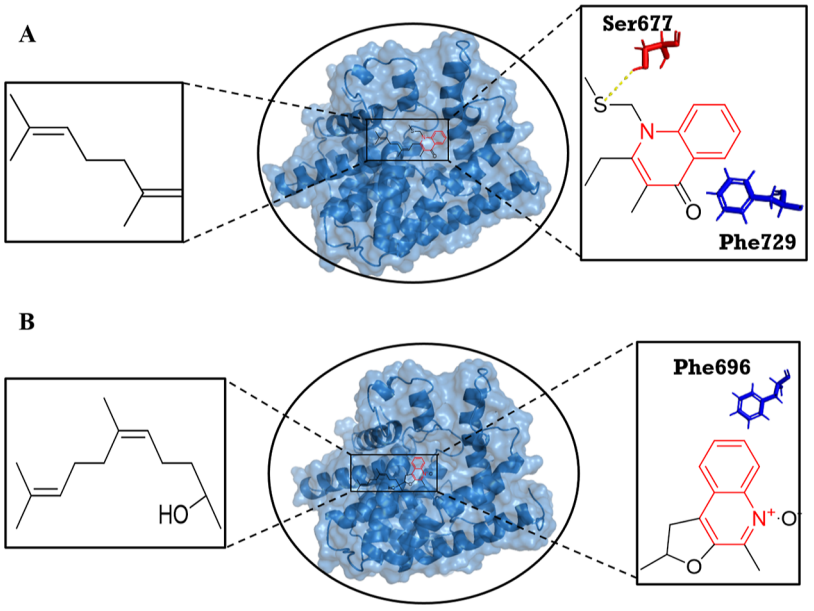

Figure 4. Molecular interactions of CJ-13536 (A) and Aurachin A (B) with PDE10A, with a focus on the major quinoline structure (at right), highlighted in red, and the remaining portion (at left), featuring their respective interactions with PDE10A. Red-colored residues are bonded by H-bonding, and blue-colored residues are bonded with pi−pi or H−pi bonding.

quinolines and 2 quinazolines are found to be inactive against PDE10A. The structural intricacy or adaptability of these compounds might obstruct the creation of a proper shape for docking. Furthermore, they might not match well with the selected binding site, leading to docking failures. Clearly, these four substances are not effective PDE10A inhibitors as they cannot efficiently engage with the target protein. This suggests that further alterations to their structures might be needed to enhance their binding strength.

Of the compounds used here, 52 quinoline and 10 quinazoline alkaloids showed docking scores higher than that of standard papaverine (Table S1) and were selected for further analysis. On the basis of the highest docking scores, drug-likeness, and pharmacokinetics analysis, seven quinolines and one quinazoline were selected for a detailed study. The quinolines include Lepadin G, Aspernigerin and CJ-13536, (1-(Methylthiomethyl)-3-methyl-2-((2*E*)-3,7-dimethyl-2,6-octenyl) quinoline-4(1*H*)-one), Aurachin A, 2-Undecyl-4(1*H*)-quinolone, Huajiaosimuline, and 3-Prenyl-4-prenyloxyquinolin-2-one, and the only quinazoline alkaloid was Isaindigotone.

The standard quinoline alkaloid papaverine showed a docking score of −6.8745 against PDE10A. The oxygen atoms of the 3,4-dimethoxybenzyl group of papaverine formed two hydrogen bonds with His525 and His567 with the bond

https://doi.org/10.1021/acsomega.3c10351
ACS Omega 2024, 9, 16262−16278

Table 1. Druggability of Quinoline and Quinazoline Alkaloids Showed a Docking Score Higher Than That of Standard Papaverine

Sr. no.	compound name	mol. wt. (g/mol)	HBD	HBA	nRotB	LogP	TPSA (Å^2)	Lipinski's rule	bioavailability score	BBB permeant (Log BB value)
	Papaverine	339.39	0	5	6	3.48	49.81	0	0.55	yes
			Quinolines							
1	LuzopeptinC	1343.31	10	26	10	2.47	481.20	4	0.17	no
2	LuzopeptinB	1385.35	9	27	12	4.51	487.27	4	0.17	no
3	Prothecan	980.97	2	16	19	5.14	251.64	4	0.17	no
4	Sandramycin	1221.32	6	18	8	6.54	357.10	5	0.17	no
5	Afeletecan	895.98	6	13	17	5.47	269.57	5	0.17	no
6	FR225659 related compound 5	750.24	7	10	16	2.75	242.79	3	0.17	no
7	Irinotecan	586.68	1	8	6	4.95	114.20	2	0.55	no
8	20-sulfonylamidine CPT derivative 22	706.76	1	10	11	4.98	163.63	2	0.17	no
9	FR225659	736.21	8	10	15	2.52	253.79	3	0.17	no
10	FR225659 related compound 4	764.27	7	10	17	3.70	242.79	3	0.17	no
11	Thiocoraline	1157.41	6	14	10	4.61	449.82	4	0.17	no
12	Sinotecan	492.48	2	9	8	2.61	145.02	2	0.56	no
13	Lurtotecan	518.56	1	9	3	4.07	106.36	2	0.55	no
14	FR225659 related compound 2	750.24	8	10	16	1.94	253.79	3	0.17	no
15	BN-80927 Elomotecan Hydrochloride	558.50	1	6	3	0.00	84.66	2	0.55	no
16	FR225659 related compound 3	720.21	7	9	15	2.27	233.56	3	0.17	no
17	20-sulfonylamidine CPT derivative 26	645.75	1	9	10	−1.44	145.13	3	0.17	no
18	7-(1-Methyl-2-oxopropyl) streptonigrin	576.55	4	11	9	3.35	200.26	4	0.11	no
19	Gimatecan	447.48	1	7	4	3.58	103.01	1	0.55	no
20	DB-67 Silatecan	478.61	2	6	3	3.50	101.65	2	0.55	no
21	20-sulfonylamidine CPT derivative 27	627.71	1	9	9	−1.36	119.83	3	0.17	no
22	antibiotic BE-22179	1061.19	6	14	6	4.61	399.22	4	0.17	no
23	Streptonigrin	506.46	4	10	6	2.44	197.18	3	0.11	no
24	Topotecan	421.45	2	7	3	2.79	104.89	1	0.55	no
25	Evocarpine	339.51	0	1	11	4.78	22.00	0	0.55	no
26	AurachinB	379.54	1	2	8	4.26	45.69	0	0.55	no
27	LepadinF	421.66	2	14	14	4.99	58.56	1	0.55	no
28	PenigequinoloneB	467.55	3	6	5	3.58	97.25	2	0.55	no
29	LepadinG	**419.64**	**2**	**4**	**13**	**5.29**	**58.56**	**0**	**0.55**	yes
30	**Aspernigerin**	**432.56**	**0**	**4**	**6**	**4.03**	**47.10**	**0**	**0.55**	yes
31	Karenitecin	448.59	1	5	4	3.99	81.42	1	0.55	no
32	Jaequinolone J1	449.54	2	5	6	2.76	77.02	1	0.55	no
33	Exatecan	435.45	2	7	1	2.75	107.44	1	0.55	no
34	1-Methyl-2-[(*Z*)-7tridecadienyl]-4(1*H*) quinolone	339.51	0	1	11	4.62	22.00	0	0.55	no
35	Belotecan	433.50	2	6	5	3.58	93.45	1	0.55	no
36	2-(Undec-1-enyl) quinolin4(1*H*)-one	311.46	1	1	10	4.46	32.86	0	0.55	no
37	AurachinC	379.54	1	2	8	5.12	42.23	1	0.55	no
38	CJ-13536	**355.54**	**0**	**1**	**7**	**3.87**	**47.30**	**0**	**0.55**	yes
39	LepadinE	421.66	2	4	14	4.99	58.56	0	0.55	no
40	1-Methyl-2-pentadecyl-4(1*H*)-quinolone	369.58	0	1	14	5.35	22.00	1	0.55	no
41	AurachinA	**395.53**	**1**	**3**	**7**	**4.02**	**54.92**	**0**	**0.55**	yes
42	Dihydroevocarpine	341.53	0	1	12	4.85	22.00	0	0.55	no
43	20-sulfonylamidine CPT derivative 25	661.72	1	9	9	−1.65	119.83	3	0.17	no
44	AurachinD	363.54	1	1	8	4.80	32.86	0	0.55	no
45	Rubitecan	393.35	1	7	2	2.15	127.24	1	0.55	no
46	2-Undecyl-4(1*H*)-quinolone	**299.45**	**1**	**1**	**10**	**4.12**	**32.86**	**0**	**0.55**	yes
47	**Huajiaosimuline**	**325.40**	**0**	**3**	**4**	**3.53**	**48.30**	**0**	**0.55**	yes
48	3-Prenyl-4prenyloxyquinolin-2-one	**297.39**	**1**	**2**	**5**	**3.37**	**42.09**	**0**	**0.55**	yes

https://doi.org/10.1021/acsomega.3c10351
ACS Omega 2024, 9, 16262−16278

Table 1. continued

Sr. no.	compound name	mol. wt. (g/mol)	HBD	HBA	nRotB	LogP	TPSA (Å^2)	Lipinski's rule	bioavailability score	BBB permeant (Log BB value)
				Quinazolines						
1	Fumiquinazoline H	485.53	2	6	2	3.09	105.56	2	0.55	no
2	FiscalinA	473.52	3	6	3	2.30	116.56	2	0.55	no
3	(+)-Nα-Quinaldyl-L-arginine	330.36	5	4	9	0.95	142.93	3	0.55	no
4	FiscalinC	487.55	3	6	3	3.11	116.56	2	0.55	no
5	Fumiquinazoline B	445.47	3	6	2	2.08	116.56	2	0.55	no
6	Fumiquinazoline I	487.55	3	6	4	2.99	116.56	2	0.55	no
7	Fumiquinazoline G	358.39	2	3	4	2.30	79.78	1	0.55	no
8	Fumiquinazoline A	445.47	3	6	2	2.08	116.56	1	0.55	no
9	Dictyoquinazol C	342.35	1	5	5	2.63	79.31	1	0.55	no
10	**Isaindigotone**	**350.37**	**1**	**5**	**3**	**3.13**	**73.58**	**1**	**0.55**	yes

distances of 2.6 and 2.2 Å, respectively (Figure 2B). These results seem consistent with the available literature.[35,36] We choose the unique binding pattern of papaverine with PDE10A (PDB ID: 2WEY) as a simultaneous contrast for further virtual screening. The Papaverine−2WEY docked complex showed a similar docking score of −6.7294 and similar binding interactions (Figure 2C). Among our top alkaloids, hydrogen bonding with His525 was also observed for Lepadin G (Figure 3A) and Huajiaosimuline (Figure S1B). Papaverine also showed hydrophobic interactions with PDE10A (PDB: 6MSA) by forming two pi-bonds, one with Phe696 by the quinoline moiety and the other with Phe729 by the unique portion, having −0.7 and −0.8 kcal/mol energy with distances of 3.77 and 3.97 Å (Figure 2B). Phe696 is one of the significant residues in the inhibition of PDE10A.[34] Among the top alkaloids in the library, Aurachin A represented the interaction with this particular residue (Figure 4B). However, the other residue, Phe729, was found in the interaction profiles of many alkaloids, namely, CJ-13536, Huajiaosimuline, 3-Prenyl-4-prenyloxyquinolin-2-one, and Isaindigotone. Many of them tend to bind more strongly than papaverine with the binding pocket of PDE10A by forming hydrogen bonds (Figures 3, 4, S1, and Table S2).

The quinoline alkaloid Lepadin G showed the highest docking score of −7.4966 by exhibiting polar interactions with PDE10A. It showed two H-bonds with His525 and Asp674 at distances of 3.17 and 3.14 Å, having energies of −6.6 and −1.0, respectively (Figure 3A). Lepadins contain a decahydroquinoline moiety with either a cis or trans configuration, and they have over 60 alkaloid members in the family. Our library included seven Lepadins (A−G) based on their significant biological activity; among them, Lepadin G was found to be a potent inhibitor as well as able to cross the blood−brain barrier. Lepadin G ([(2R,3R,4aS,5S,8aR)-5-(5-hydroxyoctyl) −2-methyl-1,2,3,4,4*a*,5,6,7,8,8*a*-decahydroquinolin-3-yl] (2*E*,4*E*)-octa-2,4-dienoate) was isolated by Carroll and co-workers from *Aplidium tabascum* Kott.[37] It has pharmacological effects that are cytotoxic to cancer cell lines and inhibit tyrosine kinase and butyrylcholine esterase activity while possessing antiparasitic characteristics. Lepadins may therefore be a promising class of marine natural materials for the design of new therapeutic drugs.[38]

Aspernigerin showed a docking score of −7.4754 by forming one polar and one nonpolar interaction with the receptor protein. It showed one H-bond with Leu675 with a distance of 3.37 Å and a binding energy of −0.9 kcal/mol. It formed one Pi-H with Tyr730 with a distance of 4.48 Å and an energy of −0.6 kcal/mol (Figure 3B). Aspernigerin (1,4-bis[2-(3,4-dihydro-2*H*-quinolin-l-yl)-2-oxoethyl] piperazine) was isolated from the extract of a culture of an endophyte in Cyndon dactylon, *Aspergillus niger* IFB-E003.[39] It has shown cytotoxic effects on tumor cell lines and has potential as a pharmaceutical or lead compound. In studies, aspernigerin demonstrated certain fungicidal, insecticidal, and herbicidal properties[40]

The top quinolines also included the quinolin-4-one moiety, CJ-13536 (1-(Methylthiomethyl)-3-methyl-2-((2*E*)-3,7-dimethyl-2,6-octenyl) quinoline-4(1*H*)-one), isolated by Dekker and co-workers in 1998 from the fermentation broth of the actinomycete Pseudonocardia sp. CL38489. CJ-13536 displayed a docking score of −7.2160 against the target protein. It showed polar interaction by forming one H-bond with Ser677 with a distance of 4.38 Å and an energy of −0.6 kcal/mol. It showed hydrophobic interaction by forming one pi−pi with Phe729 with an energy of −0.0 kcal/mol and a distance of 3.98 Å (Figure 4A). It exhibited highly selective and specific antibacterial activity against *Helicobacter pylori* with MICs up to 0.1 ng/mL, and it was less likely to disturb normal gastrointestinal microbial flora if used as an antiulcer agent.[41] Aurachin A exhibited only one pi−pi interaction with residue Phe696 (Figure 4B). Interestingly, our curated alkaloid collection included Aurachin A−D; among them, only Aurachin A had the required drug-like properties (Table 1).

2-Undecyl-4(1*H*)-quinolone exhibited a docking score of −6.9234 against PDE10A. It formed an H bond with Ser677 at a distance of 2.86 Å, similar to the H bond with the sulfur atom of Lepadin G (Figure 4A). It showed a hydrophobic interaction by forming one Pi-H with Ile692 at a distance of 4.39 Å and an energy of −0.7 kcal/mol (Figure S1A). Moreover, it formed a 6-ring pi−pi interaction involving the key residue, PHE729 (with a less negative docking score of −6.4385), at the distance and energy of 3.58 Å and −0.0 kcal/mol, respectively. While the hydrogen bond with accessible residues Ser677 and hydrophobic interaction with Ile692 may not significantly contribute to PDE10A inhibition (as they are not directly involved in cAMP/cGMP binding), similar interactions with these residues are evident in the profiles of reference PDE10 inhibitors like papaverine, Tofisopam, and Dipyridamole.[42] Also, hydrophobic interaction with Ile692 plays a pivotal role in providing stability to the inhibitor in the PDE10A active site.[43] 2-undecyl-4(1*H*)-quinolone is a reported antimicrobial metabolite that was isolated from the

https://doi.org/10.1021/acsomega.3c10351
ACS Omega 2024, 9, 16262−16278

Gram-negative sponge-associated marine bacterial strain of Pseudomonas sp. It showed activity against HIV-1,[44] *M. smegmatis*, and *M. fortuitum* (MICs 12.5−200 μM).[45]

Huajiaosimuline demonstrated a docking score of −6.9002 against the receptor protein. It showed polar interactions by forming H-bonds with His525 and Met713 with energies of −7.7 and −0.2 kcal/mol, respectively, having distances of 2.78 and 3.57 Å. It also showed hydrophobic interaction by forming pi−pi with Phe729 with an energy of −0.0 kcal/mol and a distance of 3.70 Å (Figure S1B). Huajiaosimuline was isolated from *Zanthoxylum simulans* and reported for its cytotoxic activity and antiplatelet aggregation activity.[46]

The quinazoline 3-Prenyl-4-prenyloxyquinolin-2-one has a docking score of −7.2807 against the target protein. It showed a hydrophobic interaction by forming pi−pi with Phe729 at a distance of 3.80 Å and a binding energy of −0.0 kcal/mol (Figure S2A). Isaindigotone showed a docking score of −7.0113 against the PDE10A enzyme. It showed a pi−pi interaction with Phe729 with an energy of −0.0 kcal/mol and a distance of 3.85 Å (Figure S2B). Isaindigotone (a naturally occurring vasicinone analogue) was discovered in the root of *Isaits indinatca fort* and has been suggested to have anticancer and anti-inflammatory therapeutic activity.[47] It showed superior scavenging potential for superoxide generated in the hypoxanthine/xanthine oxidase system, with an IC50 of 42.2 nM. It inhibited PGE2 and NO production in RAW 264.7 macrophages.[48]

Moreover, it was observed that more than 7 cyclic peptide compounds with the quinoline moiety exhibited docking scores lower than that of papaverine (Table S1). Cyclic peptides have several advantageous characteristics that make them appealing for use in medication development. There are currently around 40 cyclic peptide-based medicines in use.[49] The lower docking score and, therefore, superior binding affinity of cyclic peptides over those of papaverine are due to specific structural features and interactions. Luzopeptin A, for instance, with the docking score of −10.0610 kcal/mol, forms four hydrogen bonds with the target protein residues (Leu635, Ala636, Asp675, and Gln726), with three bonds involving its quinoline moieties and one with an interpeptide amino acid (Figure 5). Interestingly, it interacted with a critical residue, i.e., Gln726, in the inhibition of PDE10A. The dual quinoline ends of cyclic peptides, compared to linear compounds with a single quinoline moiety and an additional bond with an amino acid, increase the total hydrogen bonding, enhancing target protein affinity. These interactions, combined with the cyclic structure's flexibility and complementarity to the receptor site, contribute to the increased efficacy of cyclic peptide compounds. These findings can guide the design of novel quinoline and quinazoline scaffolds as targeted PDE10A inhibitors with enhanced affinity and specificity, leveraging the structural advantages of cyclic peptides for improved drug efficacy.

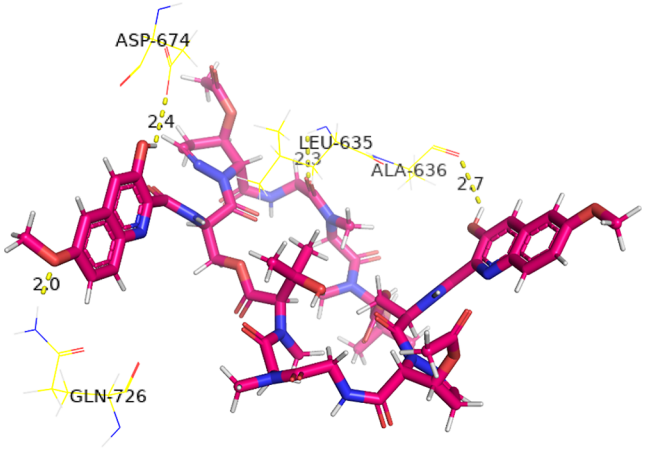

Figure 5. Molecular interactions of Luzopeptine A with PDE10A (PDB: 6MSA).

Many derivatives of camptothecin are predicted to have activity higher than that of papaverine via molecular docking and MD simulations. A successful Camptothecin derivative, Irinotecan (CPT-11), approved as a drug for cancer treatment, was chosen to indirectly demonstrate the reliability of the prediction method.[50] Its superior docking score of −7.4395 and many strong polar interactions (Figure 6) provide computational evidence for the higher activity of camptothecin derivatives than that of papaverine. This confirms the reliability of our methodology and excludes false positives. This validation further strengthens the robustness of our findings and enhances the confidence in our computational approach.

The quinoline ring structure, which predominates in our reference molecule, and the similar structural moiety of quinazoline were the focus of our study. The well-established interaction profile of the quinoline moiety of papaverine has a significant effect on the ligand selection process. Both the quinoline and quinazoline moieties showed unique interactions that are essential to the compound's overall activity. Distinct from these alkaloid structures, the remaining portion of the ligand demonstrated fewer but distinct interactions that enhance the compound's activity. Knowing how the alkaloid moiety and the remaining ligand structure work together symbiotically offers important information about possible directions for compound optimization and additional research.

3.4. Essential Pharmacophores for PDE10A. The objective was to strategically identify the distinct pharmacophoric motifs, predominantly based on a quinoline/quinazoline scaffold. This approach aimed to optimize their affinity and efficacy in inhibiting PDE10A, thus enhancing their potential as pharmacological agents. Focusing on compound CJ-13536, the inclusion of a sulfur atom provides an interesting feature. It not only augments the compound's hydrogen bonding capabilities but also introduces a unique element that could potentially improve selectivity and potency by offering an additional interaction point not commonly found in similar compounds. We introduced all of the pharmacophoric features of the quinoline and quinazoline scaffold in CJ-13536 that were observed in the top compounds to create a common pharmacophore. The features identified (Figure 7) G1 and G6, both with the "Aro" descriptor for aromaticity with the radii of 0.50 and 0.62, respectively, highlighting the importance of aromatic interactions, which are characteristic of the quinoline scaffold. These features contribute to $\pi-\pi$ stacking interactions, which are essential for binding to the target protein. The presence of "Hyd" in G6, alongside "Aro", suggests a region in the compound that can participate in both hydrophobic interactions and $\pi-\pi$ stacking, offering a dual role in enhancing the binding affinity. G7, with a larger radius of 0.89 and labeled "Hyd", points to a significant hydrophobic region, further emphasizing the compound's ability to engage with hydrophobic pockets of the enzyme. G10, labeled "Acc" with a radius of 0.50, indicates a hydrogen bond acceptor site,

https://doi.org/10.1021/acsomega.3c10351
ACS Omega 2024, 9, 16262−16278

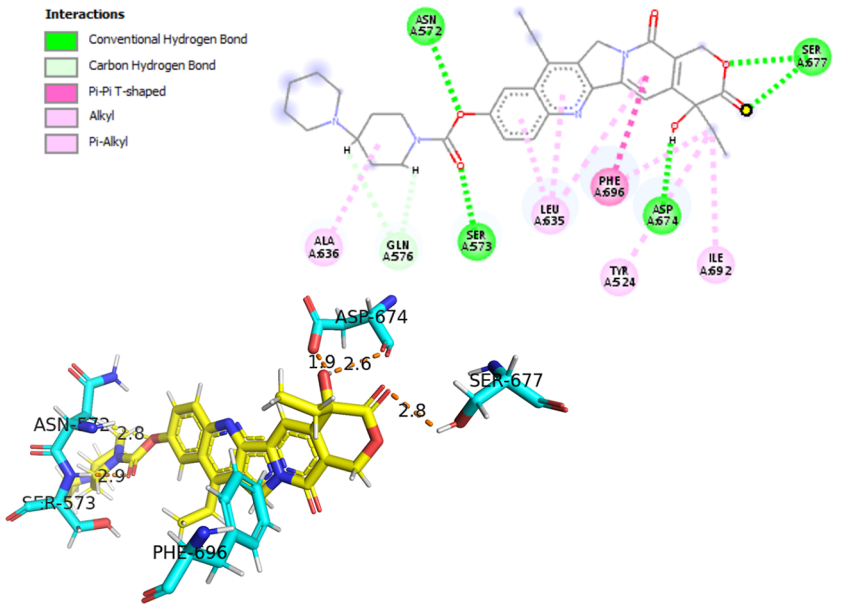

Figure 6. Molecular interaction of Irinotecan (CPT-11) (yellow) with PDE10A residues (cyan).

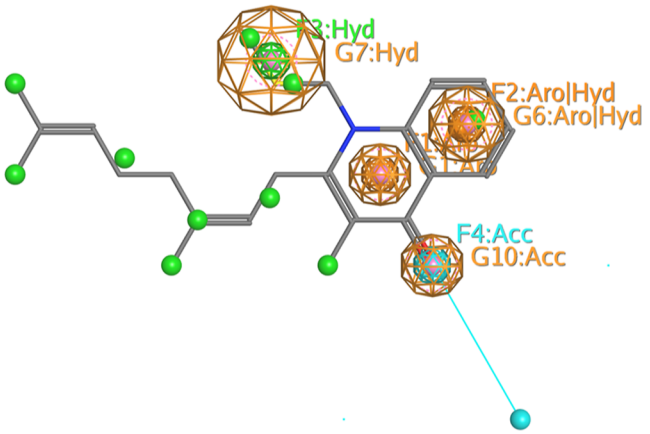

Figure 7. Critical pharmacophoric features essential for the inhibition of PDE10A. The features identified with variable radii are G1, G6, G7, and G10, with the descriptors of Aro, Hyd, and Acc indicating the aromatic, hydrophobic, and hydrogen bond acceptor site, respectively.

crucial for forming specific interactions with hydrogen bond donors within the active site of PDE10A. Highlighting these pharmacophoric features elucidates the intricate relationship between the compound and its biological target, emphasizing the significance of each interaction site and spatial configuration in achieving the intended therapeutic outcome.

3.5. CNS-Active Drug Criteria. Many studies have been performed based on the physicochemical characteristics of commercially available CNS-active drugs. Their findings take into account not only brain penetration but also the overall ADME and specifications for an effective CNS drug candidate.[51] SwissADME and pkCSM are popular web-based platforms that provide reliable predictive models for the pharmacokinetics and pharmaceutical properties of a molecule. Further screening of the hits was performed based on the CNS-active drug criteria by using these tools. The 52 quinoline and 10 quinazoline alkaloids that showed a higher docking score than that of the standard alkaloid were selected for drug-likeness analysis (Table 1), while four quinolines did not follow any property.

Biological membranes are selective barriers that allow for specific lipophilic compounds to cross them. A compound's lipophilicity affects its membrane passage and drug potential. The descriptor log *P*0/*w* is usually used to represent the permeation, which is evaluated through the octanol−water partition coefficient of the unionized molecule. Various log *P* predictive models are used to denote the values of log *P*0/*w*, namely, XLOGP3, iLOGP, WLOGP, MLOGP, and Silicos-IT log *P*, whereas the consensus log *P* is the arithmetic mean of these five models. CNS-active drugs ideally have a consensus log *P* of 2−5.[52] The higher and poor consensus log *P* values of quinolines, 3, 4, 5, 17, 21, 29, 37, 40, and 43, for consensus log *P* indicate that these drugs do not follow the CNS-active drug criteria due to the higher or lower lipophilicity (Table 1). The remaining hits meet the specification for being the drug pertaining to lipophilicity, ensuring their capacity to effectively traverse the blood−brain barrier. This property enhances their therapeutic potential for addressing brain diseases while minimizing the risk of adverse side effects.

Molecular weight is another important property for quick evaluation of drug-likeness. The permeability and solubility of a compound can be attributed to its molecular weight. Moreover, the solubility of a compound in an aqueous system decreases with an increase in size. The molecular weight of a compound should be < 450 g/mol in accordance with Lipinski's rule of five for CNS-active drugs.[52] Quinolines 19, 24−42, and 44−48 and quinazolines 3, 5, and 710 have molecular weights in accordance with the Lipinski rule (Table 1).

After absorption into the bloodstream, the drug is transported to its target site. Polarity is a factor that contributes to the transport efficiency of a drug and is described by the topological molecular polar surface area (TPSA). The values of TPSA should be less than 60 Å^2. Quinolines 25−27, 29, 30, 34, 36, 42, 44, 46, and 47 show polarity according to the rule (Table 1).

https://doi.org/10.1021/acsomega.3c10351
ACS Omega 2024, 9, 16262−16278

Table 2. Pharmacokinetic Properties and Drug−Drug Interactions of Top Alkaloids

Sr. no.	compound	GI absorption	CNS activity	Pgp substrate	CYP1A2 inhibitor	CYP2C19 inhibitor	CYP2C9 inhibitor	CYP2D6 inhibitor	CYP3A4 inhibitor
ref.	Papaverine	high	−2.348	no	yes	yes	yes	no	yes
1	LepadinG	high	−2.362	yes	no	no	no	no	no
2	Aspernigerin	high	−1.375	yes	no	no	no	yes	no
3	CJ-13536	high	−1.845	no	yes	yes	yes	no	no
4	AurachinA	high	−1.792	yes	no	no	no	yes	no
5	2-Undecyl-4(1*H*)-quinolone	high	−1.633	yes	yes	yes	yes	no	no
6	Huajiaosimuline	high	−1.996	no	yes	yes	no	no	no
7	3-Prenyl-4-prenyloxyquinolin -2-one	high	−1.379	yes	yes	yes	yes	no	no
8	Isaindigotone	high	−2.225	no	yes	yes	yes	no	yes

The flexibility of a molecule is directly related to its oral bioavailability. Moreover, a highly flexible molecule has more chances of rearrangements in the structure and more chances of binding to the target. The permissible limit of flexibility is less than 10 rotatable bonds, in accordance with Lipinski's rule of five (RO5) for CNS-active drugs. Quinolines 2, 3, 5, 6, 8, 9, 14, 16, 25, 27, 29, 34, 39, 40, and 42 did not meet this criterion. Other than these compounds, all quinolines and quinazolines reside within the admissible limit of molecular flexibility. Lipinski's RO5 proposes that the number of hydrogen bond acceptors and donors should be less than 10 and 3, respectively. All of the tested alkaloids except 15 quinolines and all of the quinazoline alkaloids followed the rule (Table 1).

Although 23 quinolines and 5 quinazolines were following the Lipinski rule of CNS-active drugs (log *P*: 2−5, MW: < 450 g/mol, TPSA: < 60 Å^2, nRot: < 10, nHBA: < 10, and nHBD: < 3) with zero or one violation (Table 1), BBB permeability was included to further refine the selection of lead alkaloids in the study. SwissADME results indicated the BBB penetration of 7 out of 48 quinoline alkaloids and 1 out of 10 quinazoline alkaloids. These 7 quinolines (Lepadin G, Aspernigerin, CJ-13536, Aurachin A, 2-Undecyl-4(1*H*)-quinolone, Huajiaosimuline, and 3-Prenyl-4-prenyloxyquinolin-2-one) and 1 quinazoline, namely, Isaindigotone, which are BBB permeable also follow the Lipinski rule of CNS-active drugs (Table 1). The BBB is a unique barrier of the CNS that contains microvascular endothelial cells. These cells control the influx and efflux through the brain.[53] BBB penetration is the required property in this study as the target enzyme PDE10A resides inside the brain.

3.6. Pharmacokinetics and Drug−Drug Interactions. Based on the criteria for CNS-active drugs and BBB permeability, certain compounds have been selected for further in-depth analysis. All of the top alkaloids also showed high gastrointestinal absorption (Table 2). Another significant property of a brain drug is P-glycoprotein (Pgp). Pgp is expressed on the plasmatic membrane of endothelial cells in the BBB. It is the efflux transporter in the BBB that pumps out many drugs, acting as a protective mechanism. Among the top alkaloids, CJ-13536, Huajiaosimuline, and Isaindigotone were non-Pgp substrates (Table 2). These alkaloids can be better retained in the brain, offering improved therapeutic efficacy as drugs for neurodegenerative disorders, particularly PD, at potentially reduced doses.

The primary human metabolizing enzyme system is called cytochrome P450 (CYP), and it is responsible for the metabolism of various drugs, carcinogens, mutagens, and alcohols. The CYP enzymes typically account for 70−80% of phase I metabolism and have the role of biotransforming the lipophilic medications into polar metabolites to be eliminated by the kidneys.[54] CYP1A2, CYP2C9, CYP2C19, CYP2D6, and CYP3A4 are important drug-metabolizing enzymes. The analysis of the eight compounds revealed a variety of inhibitory patterns on five cytochrome P450 enzymes. Alkaloids, namely, CJ-13536, 2-Undecyl-4(1*H*)-quinolone, 3-Prenyl-4-prenyloxyquinolin-2-one, and isaindigotone, inhibited CYP1A2 and CYP2C19, with the first three also inhibiting CYP2C9. In contrast, aspernigerin and aurachin A specifically inhibited CYP2D6, and isaindigotone distinctly inhibited CYP3A4 (Table 2).

Compounds with broader inhibitory profiles, such as CJ-13536, 2-Undecyl-4(1*H*)-quinolone, and 3-Prenyl-4-prenyloxyquinolin-2-one, pose a predicted risk for drug−drug interactions, particularly with CNS-active drugs, due to their potential to increase the plasma concentrations of multiple drugs metabolized by these enzymes. This rise can amplify therapeutic effects or result in toxicity. Although it should be considered that the standard compound is also a potential inhibitor of these cytochromes, conversely, aspernigerin and aurachin A, with their selective inhibition of CYP2D6 (Table 2), may offer a safer profile in combination therapies. Their specificity suggests a reduced risk of widespread drug−drug interactions, enabling a more predictable and manageable pharmacological response. This selectivity could be especially beneficial for patients in polypharmacy, where the complexity of interactions can be challenging to navigate. Isaindigotone is of particular interest, given its unique inhibition of CYP3A4, an enzyme known for metabolizing a vast array of medications.[54] Its inhibitory effect determines the necessity for cautious usage when coadministered with drugs metabolized by CYP3A4 to avoid unexpected increases in drug concentrations and potential adverse effects.

In brief, while broad-spectrum inhibitory compounds are crucial for understanding potential drug−drug interactions, compounds with selective inhibition patterns represent more targeted pharmacological therapies, balancing efficacy and safety. These findings emphasize the nuanced approach needed in evaluating and managing drug−drug interactions, particularly for CNS-active drugs, and provide a foundation for more individualized and safe therapeutic strategies.

3.7. Pharmacological Parameters of the Top Alkaloids. The time of elimination ($T_{1/2}$) and clearance (CL) are the primary metrics pertaining to the elimination process.[55] The first one ($T_{1/2}$) shows how long it takes for the drug's plasma concentration to drop to half of its starting value, which is the rate at which elimination happens at the slowest. For first-order reactions, the half-life can be found using the

https://doi.org/10.1021/acsomega.3c10351
ACS Omega 2024, 9, 16262−16278

Table 3. Toxicology and Medicinal Chemistry Analysis of Top Alkaloids

Sr. no.	compound	AMES toxicity	hepatotoxicity	PAINS alert	lead-likeness	synthetic accessibility
ref.	Papaverine	no	yes	0	0	2.62
1	LepadinG	no	yes	0	no; 3 violations	5.59
2	Aspernigerin	no	yes	0	no; 1 violation	3.11
3	CJ-13536	no	yes	0	no; 2 violations	3.66
4	AurachinA	yes	no	1	no; 2 violations	4.58
5	2-Undecyl-4(1*H*)-quinolone	no	yes	0	no; 2 violations	2.77
6	Huajiaosimuline	no	yes	0	yes	4.01
7	3-Prenyl-4-prenyloxyquinolin-2-one	yes	yes	0	no; 1 violation	2.98
8	Isaindigotone	no	yes	0	no; 1 violation	3.24

equation $T_{1/2}$ = 0,693/k, where k is the elimination constant. Clearance rates are categorized as high (>15 mL/min/kg), moderate (5−15 mL/min/kg), and low (<5 mL/min/kg). Half-life values are classified as long (>3 h) or short (<3 h). The output in Table S3 represents the probability of a long half-life.

Aspernigerin, Aurachin A, Isaindigotone, CJ-13536, and 3-prenyl-4-prenyloxyquinolin-2-one have moderate clearance in the range 6−12 mL/min/kg (Table S3). Their moderate plasma clearance rates suggest a balanced elimination rate from the body. The low clearance observed for Lepadin G, Huajiaosimuline, and 2-undecyl-4(1*H*)-quinolone indicates that these alkaloids are eliminated from the body at a slower rate. This suggests the potential for a long-lasting therapeutic effect when these compounds are administered, making them suitable for treating chronic conditions. However, it also highlights the need for careful dosing and monitoring to prevent potential accumulation and ensure safe and effective use.

Isaindigotone stands out with a high probability of having a half-life greater than 3 h (Table S3). This indicates that Isaindigotone tends to persist in the body for an extended period, which can have implications for its pharmacological activity and potential effects. On the contrary, all the other top alkaloids in the study show a high probability of having a half-life of less than 3 h, suggesting that they are rapidly eliminated from the body. These findings have important implications for the pharmacokinetics and dosing regimen of these alkaloids in potential medical applications.

3.8. Toxicology and Medicinal Chemistry. The toxicity of the top 8 compounds was estimated using the pkCSM server and compared with the standard (Table 3). The AMES test predicted the toxicity of the drugs. Only Aurachin A (quinoline 4) and 3-Prenyl-4-prenyloxyquinolin-2-one showed toxicity in the AMES test, indicating the capability of genetic mutations. The rest of the alkaloids do not show toxicity. Hepatotoxicity estimates the ability of drugs to cause damage to the liver. All the alkaloids showed standard predicted hepatotoxicity in toxicological tests except Aurachin A (Table 3).

We analyzed the different medicinal properties, such as reactivity, potent response, and biosynthetic availability, of top hits in biological assays using the SwissADME server (Table 3). PAINS (pan-assay interference compounds) are promiscuous or hitter compounds that contain substructures that exhibit potent activity in biological assays regardless of the main target.[56] None of the alkaloids showed an alert against PAINS except Aurachin A. Synthetic accessibility is the ease of synthesis of compounds. All the top alkaloids showed an acceptable score for synthetic accessibility; however, Lepadin G showed the highest score among the top alkaloids and the standard used in this study (Table 3).

3.9. Toxicity End-Points. In terms of carcinogenicity, immunotoxicity, mutagenicity, and cytotoxicity, the top quinoline alkaloids demonstrated better overall toxicity profiles, with inactivity across all the toxicity end-points, making them potentially safer options (Table S4). However, caution is needed with Lepadine G and CJ-13536 due to their immunotoxicity and cytotoxicity, respectively. In contrast, the quinazoline alkaloid Isaindigotone displayed a poorer toxicity profile compared with that of the reference alkaloid (Papaverine), which suggests safety concerns.

3.10. Predicted Biological Targets. In the fields of pharmacology and computer-aided drug design, Swiss Target Prediction software is a well-known tool. Using a similarity to known ligands, this tool helps researchers predict the most probable protein targets for a small molecule. As it sheds light on potential mechanisms of action, off-target effects, and potential therapeutic applications of novel compounds, this is incredibly helpful in the drug discovery process. Early identification of these protein targets can help conserve time and money while directing future research. We analyzed and discussed the top 15 predicted targets of each alkaloid and provided details on the top five.

The Swiss target prediction results for Lepadin G revealed a list of potential protein targets with which it might interact. The probability score, as indicated in Table 4, is 0.1 for each of the listed targets. This probability suggests a lower likelihood of interaction between Lepadin G and the predicted proteins. Also, these targets are not directly implicated in PD. Among the top 15 targets, 33% were from the family of G protein-coupled receptors (Figure 8A). The top targets included the gamma−secretase complex, apoptosis regulators (Bcl-X and Bcl-2), melanin-concentrating hormone receptor 1, and beta-secretase 1 (BACE1).

The associated probability scores of Aspernigerin range from 0.10 to 0.13, indicating a lower likelihood of Aspernigerin binding and interacting with these proteins (Table 4). 60% of the predicted proteins were indicated to belong to the family of G protein-coupled receptors (Figure 8B). Similarly, the maximum predicted targets for CJ-13536, Huajiaosimuline, and 3-Prenyl-4-prenyloxyquinolin-2-one, given as 40, 46.7, and 40%, respectively, belonged to the family of G protein-coupled receptors (Figures 8C, S3B,C). Aspernigerin demonstrated an affinity for dopamine receptors. Dopamine receptors play a key role in the regulation of mood, reward, and motor control, among other brain activities. Their dysregulation has been linked to a number of illnesses, including PD and schizophrenia.[8] The potential applications of Aspernigerin with numerous dopamine receptors, i.e., D2, D3, and D4,

https://doi.org/10.1021/acsomega.3c10351
ACS Omega 2024, 9, 16262−16278

Table 4. Swiss Target Prediction Analysis of the Top Alkaloids

target	common name	target class	probability*
	Lepadin G		
gamma−secretase	PSEN2 PSENEN NCSTN APH1A PSEN1 APH1B	protease	0.10
apoptosis regulator Bcl-X	BCL2L1	other ion channel	0.10
apoptosis regulator Bcl-2	BCL2	other ion channel	0.10
melanin-concentrating hormone receptor 1	MCHR1	family A G protein-coupled receptor	0.10
beta-secretase 1	BACE1	protease	0.10
	Aspernigerin		
dopamine D2 receptor	DRD2	family A G protein-coupled receptor	0.13
dopamine D4 receptor	DRD4	family A G protein-coupled receptor	0.13
serotonin 1a (5-HT1a) receptor	HTR1A	family A G protein-coupled receptor	0.10
melatonin receptor 1A	MTNR1A	family A G protein-coupled receptor	0.10
dopamine D3 receptor	DRD3	family A G protein-coupled receptor	0.10
	CJ-13536		
11-beta-hydroxysteroid dehydrogenase 1	HSD11B1	enzyme	0.09
voltage-gated T-type calcium channel alpha-1*H*subunit	CACNA1H	voltage-gated ion channel	0.09
melatonin receptor 1A	MTNR1A	family A G protein-coupled receptor	0.09
melatonin receptor 1B	MTNR1B	family A G protein-coupled receptor	0.09
cannabinoid receptor 1 (by homology)	CNR1	family A G protein-coupled receptor	0.09
	Aurachin A		
protein farnesyltransferase	FNTA FNTB	enzyme	0
thrombin and coagulation factor X	F10	protease	0
macrophage colony stimulating factor receptor	CSF1R	kinase	0
C−C chemokine receptor type 3	CCR3	family A G protein-coupled receptor	0
C−C chemokine receptor type 5	CCR5	family A G protein-coupled receptor	0
	2-undecyl-4(1*H*)-quinolone		
cathepsin (V and K)	CTSV	protease	1
cathepsin L	CTSL	protease	1
poly [ADP-ribose] polymerase-1	PARP1	enzyme	0.11
sodium-dependent proline transporter	SLC6A7	electrochemical transporter	0.11
acetyl-CoA carboxylase 2	ACACB	ligase	0.11
	Huajiaosimuline		
melatonin receptor 1B	MTNR1B	family A G protein-coupled receptor	0.10
melatonin receptor 1A	MTNR1A	family A G protein-coupled receptor	0.10
tyrosine-protein kinase receptor FLT3	FLT3	kinase	0.10
serine/threonine-protein kinase PIM1	PIM1	kinase	0.10
Bcl2-antagonist of cell death (BAD)	BAD	other cytosolic protein	0.10
	3-Prenyl-4-prenyloxyquinolin-2-one		
adenosine A3 receptor	ADORA3	family A G protein-coupled receptor	0.11
metabotropic glutamate receptor 5 (by homology)	GRM5	family C G protein-coupled receptor	0.11
proteinase-activated receptor 1	F2R	family A G protein-coupled receptor	0.11
G-protein coupled receptor kinase 2	GRK2	kinase	0.11
serotonin 6 (5-HT6) receptor	HTR6	family A G protein-coupled receptor	0.11
	Isaindigotone		
arachidonate 5-lipoxygenase	ALOX5	oxidoreductase	1
serine/threonine-protein kinase/endoribonuclease IRE1	ERN1	enzyme	0.10
receptor protein-tyrosine kinase erbB-2	ERBB2	kinase	0.10
epidermal growth factor receptor erbB1	EGFR	kinase	0.10
serine/threonine-protein kinase Nek1	NEK1	kinase	0.10

indicate its potential for altering dopaminergic neurotransmission. Aurachin A showed a very low probability of interacting with the biological targets, which reduces the possibility of off-target side effects and guarantees a more effective and consistent therapeutic response. However, according to its overall biological activity profile, 53% of its predicted proteins were indicated to belong to the family A G protein-coupled receptors (Figure 8D).

The compound CJ-13536 shows multitarget binding to several proteins. It interacts with HSD11B1, related to cortisol metabolism,[57] and CACNA1H, affecting neuronal activity.[58] Although with very low probability (0.09) (Table 4), its affinity for melatonin receptors (MTNR1A and MTNR1B) is noteworthy, given the sleep and circadian rhythm issues in PD.[59] Additionally, its binding to the cannabinoid receptor 1 (Table 4) hints at targeting depression in PD and providing neuroprotective roles in PD.[60]

For 2-undecyl-4(1*H*)-quinolone, the top 15 targets were enzymes, proteases, and G protein-coupled receptors, each with a 20% probability of being the target (Figure S3A). It demonstrated notable affinity toward cathepsin (V and K) and cathepsin L, with values registered at 1 (Table 4). This is

https://doi.org/10.1021/acsomega.3c10351
ACS Omega 2024, 9, 16262−16278

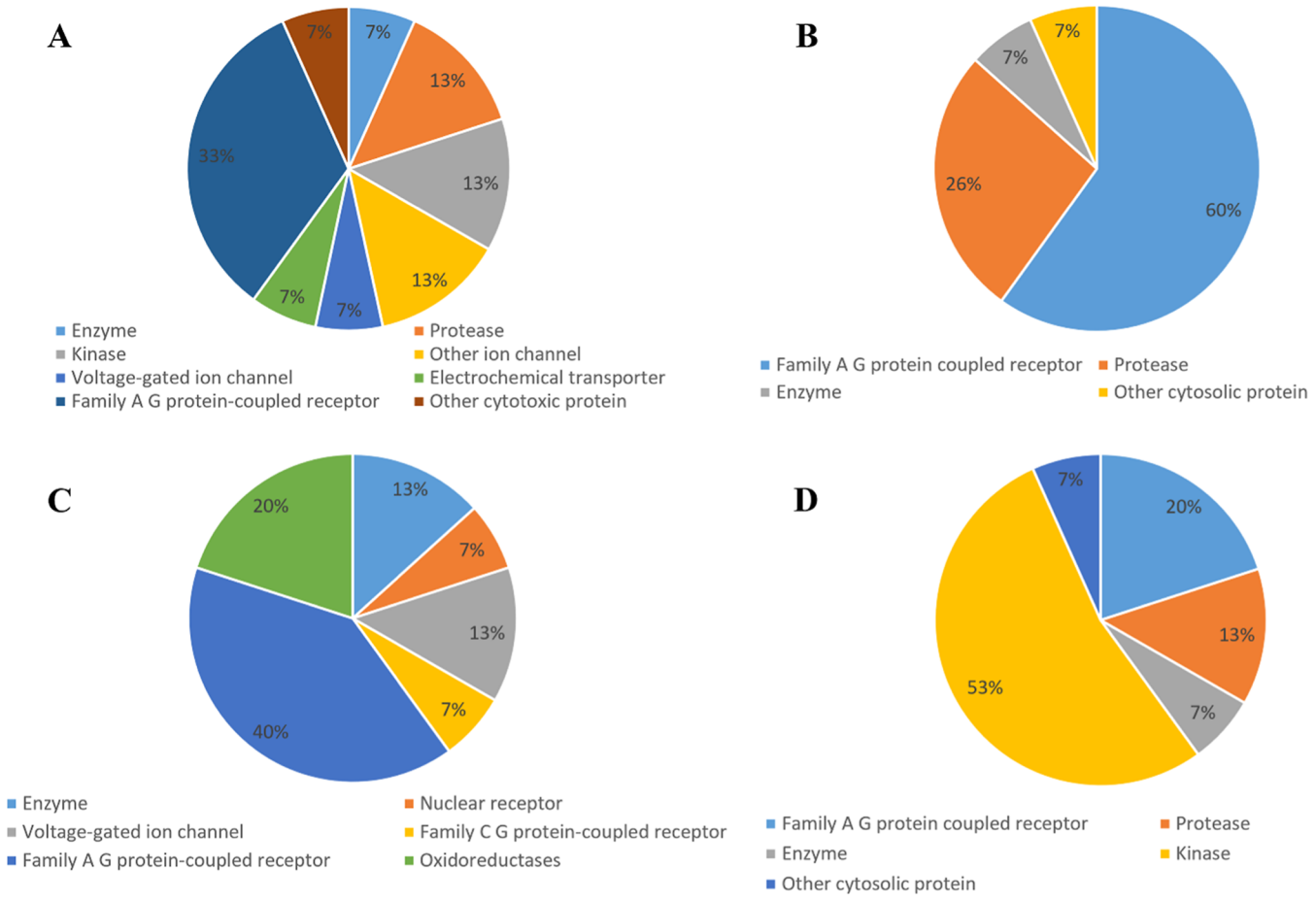

Figure 8. Pi charts illustrating the affinity of Lepadin G (A), Aspernigerin (B), CJ13536 (C), and Aurachin A (D) for various biological targets. Each colored segment in the chart represents a specific biological target, and the size of the segment corresponds to the affinity of the alkaloids for that target.

significant given the emerging understanding of cathepsins in neurodegenerative disorders.[61] Although direct links between cathepsins and PD are still under investigation, the dysregulation of these proteases can influence various pathological processes in the brain.[61]

Huajiaosimuline displayed a uniform affinity (0.10) for several targets (Table 4). It interacted with melatonin receptors 1B and 1A, which are implicated in circadian rhythm regulation, a potential factor in neurodegenerative diseases like PD.[59] Moreover, its interaction with the apoptosis regulator Bcl2-antagonist of cell death (BAD) hints at potential neuroprotective properties. The exact relevance of these interactions to PD warrants further study.

3-Prenyl-4-prenyloxyquinolin-2-one displayed a consistent affinity (0.11) for several receptors (Table 4). It interacted with the serotonin 6 (5-HT6) receptor, which is significant as serotonin is a key player in neural signaling related to PD.[62] Its association with the metabolite glutamate receptor 5 (by homology) suggests potential roles in neurodegenerative signaling pathways. Experimental data shows that modulating these receptors can enhance the motor symptoms of PD and reduce L-DOPA-induced dyskinesia, which is achieved by balancing the excitatory and inhibitory signals in the basal ganglia.[63]

Lastly, for Isaindigotone, the top 15 targets were kinase- and G protein-coupled receptors, each with a 20% probability of being the target (Figure S3D). Isaindigotone demonstrated notable affinity for Arachidonate 5-lipoxygenase (ALOX5) and multiple kinases, including IRE1, ERbB-2, ERbB1, and Nek1 (Table 4). Its interaction with ALOX5 suggests a potential strategy for treating PD by preventing ferroptosis in dopaminergic neurons.[64]

The lead compounds displayed diverse interactions with biological targets crucial to the pathophysiology of PD. Their affinity with dopamine and melatonin receptors suggests a potential for modulating dopaminergic neurotransmission and addressing circadian rhythm disturbances commonly observed in PD. The strong interaction with cathepsins underscores the evolving understanding of these enzymes in neurodegenerative mechanisms. Furthermore, the potential modulation of cellular signaling pathways suggests a multifaceted therapeutic approach.

3.11. Temporal Dynamic Mapping. For molecular dynamics simulations, Schrodinger LLC's Desmond software was employed. The simulation time was 30 ns for all three alkaloid complexes: Aspernigerin PDE10A, Isoindigotone PDE10A, and Lepadin GPE10A. The reference frame backbone is used to align each protein frame before the atom selection is used to compute the rmsd. For the purpose of interpreting the conformational stability and dynamic characteristics from the initial configuration to the final state, the rmsd in the bound and unbound states of the alkaloids and proteins was computed and displayed as a histogram against the protein's Ca atoms (Figure 9). Small departures from the

https://doi.org/10.1021/acsomega.3c10351
ACS Omega 2024, 9, 16262−16278

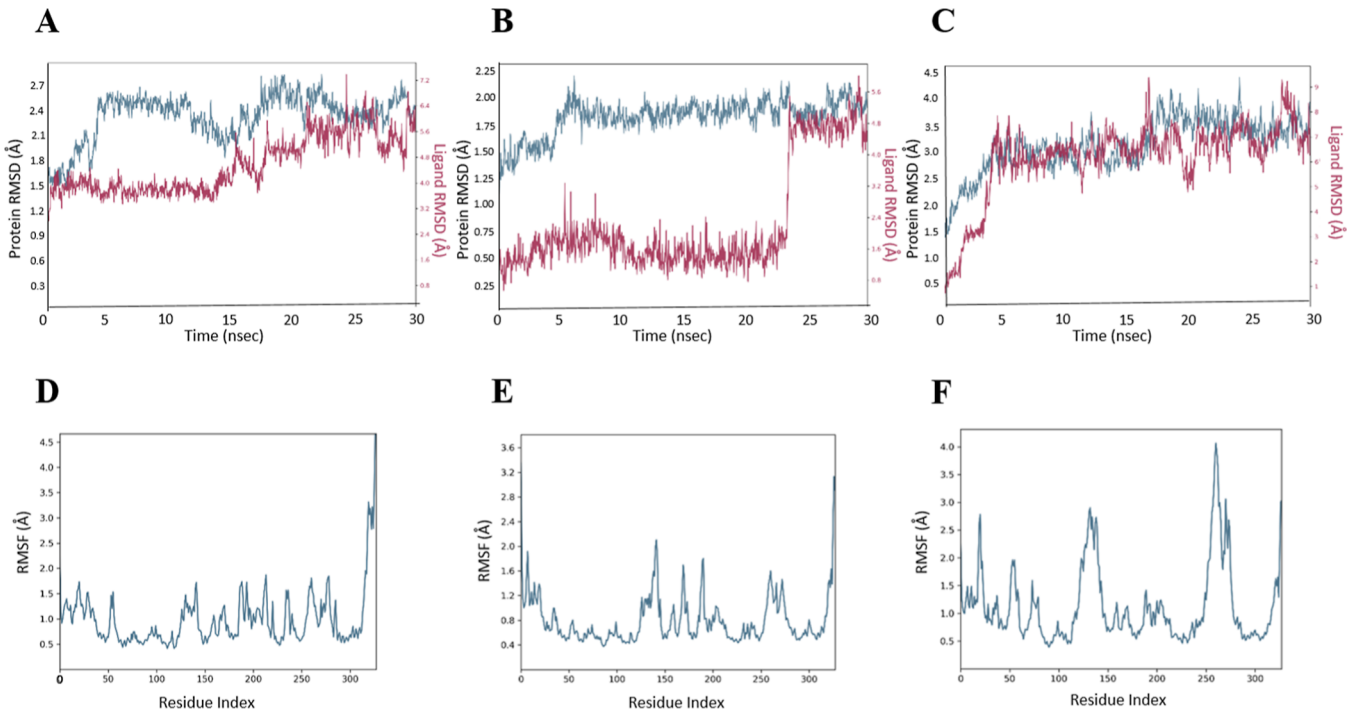

Figure 9. rmsd and rmsf plots for top alkaloids and PDE10A complexes: (A) rmsd plot for the Aspernigerin−PDE10A complex; (B) rmsd plot for the Isaindigotone−PDE10A complex; (C) rmsd plot for the Lepadin G−PDE10A complex; protein rmsd is shown in blue and ligand rmsd is shown in red color (D). rmsf plot for the Aspernigerin−PDE10A complex; (E) rmsf plot for the Isaindigotone−PDE10A complex; (F) rmsf plot for the Lepadin G−PDE10A complex.

rmsd curve suggest that the docked complex is stable and vice versa. This is the situation in the instance where PDE10A is in complex with Aspernigerin, Isaindigotone, and Lepadin G.

In the case of the Aspernigerin−PDE10A complex, the rmsd calculated was 2.7 ± 1 Å and showed sudden variations at 5 and 15 ns (Figure 9A). The rmsd of Isoindigotone PDE10A showed the most stability among the three, with a slight variation at 5 ns (Figure 9B). The rmsd of the Isaindigotone and Lepadin G complexes with PDE10A was calculated as 2.35 ± 1 and 4.5 ± 1 Å, respectively. No significant variations were identified in the calculated rmsd of the Lepadin G−PDE10A complex (Figure 9C). The rmsd plots of all three alkaloid complexes indicate their stability. The presence of naturally flexible regions can be the reason for the observed increased fluctuations in the rms values in the complexes. This noticeable fluctuation pattern supports the idea of structural dynamics in this situation and is in line with the results of earlier research.[65]

The ligand rmsd represents the stability of the alkaloids with respect to PDE10A and its binding pocket. It is possible that the ligand has diffused away from its original binding site if the values are noticeably greater than the protein's rmsd. All three alkaloid and PDE10A complexes demonstrated lower ligand values than the protein (Figure 9A−C).

The local alterations along the protein chain can be characterized using rmsf. In the rmsf plots, regions of the protein that fluctuate the most during the simulations are indicated by peaks. Therefore, we performed the residual flexibility analysis to better understand the stability of the formed complexes, which indicated that all three alkaloid and PDE10A complexes have lower values of flexibility, which confirms our analysis (Figure 9D−F).

4. CONCLUSIONS

The results of this study demonstrate the potential of quinoline and quinazoline alkaloids as PDE10A inhibitors, providing a promising direction for the therapeutic approaches to PD. Seven cyclic peptides, those featuring the quinazoline/quinazoline moiety at both termini, were of the best interest based on notably enhanced docking scores compared to those of the remaining alkaloids within the screened library, but they did not follow the standard CNS-active drug criteria. The leading alkaloids, namely, Lepadin G, Aspernigerin, CJ-13536, Aurachin A, 2-Undecyl-4(1*H*)-quinolone, Huajiaosimuline, 3-Prenyl-4-prenyloxyquinolin-2-one, and Isaindigotone, stick to the standards of CNS-active drugs, indicating their potential for CNS-targeted treatments. Huajiaosimuline emerged as a dominant alkaloid due to its alignment with lead-likeness in addition to CNS-active criteria. Moreover, the potential applications of Aspernigerin with numerous dopamine receptors indicate its potential to alter dopaminergic neurotransmission, which has been linked to a number of illnesses, including PD. Notably, most alkaloids were associated with G protein-coupled receptors, emphasizing their significance in PD therapy. Essential pharmacophores of the focused scaffold along with the unique sulfur atom presented the significant interaction sites and spatial configurations in achieving the intended enzyme inhibition. All quinoline alkaloids showed better toxicity end-points than the standard. Additionally, the selected alkaloid MD simulation results confirmed their stability in the binding pocket of PDE10A. Collectively, these results indicate that the selected drug-like quinoline and quinazoline alkaloids may offer a comprehensive approach to targeting multiple facets of PD in addition to their affinity for PDE10A. However, our findings are preliminary, and further experimental validation may offer a great opportunity to

https://doi.org/10.1021/acsomega.3c10351
ACS Omega 2024, 9, 16262−16278

explore the potential of these alkaloids in developing a potent drug against PD.

■ ASSOCIATED CONTENT

Supporting Information

The Supporting Information is available free of charge at https://pubs.acs.org/doi/10.1021/acsomega.3c10351.

> Library of biologically active quinoline and quinazoline alkaloids; interaction profile of top quinoline and quinazoline alkaloids; excretion parameters of the top alkaloids; toxicity end-point prediction and probability of the top alkaloids; molecular interactions of 2-Undecyl-4(1*H*)-quinolone and Huajiaosimuline with PDE10A with the focus on the major quinoline structure (at right), highlighted in red, and the remaining portion (at left) featuring their respective interactions with the PDE10A; red-colored residues bonded by H-bond and blue-colored residues bonded with pi−pi or H−pi bonding; molecular interactions of 3-Prenyl-4-prenyloxyquinolin-2-one and Isaindigotone with PDE10A with the focus on the major quinoline structure (at right), highlighted in red, and the remaining portion (at left) featuring their respective interactions with the PDE10A; and blue-colored residues bonded with pi−pi or H−pi bonding (PDF)

■ AUTHOR INFORMATION

Corresponding Authors

Mohibullah Shah − *Department of Biochemistry, Bahauddin Zakariya University, Multan 66000, Pakistan;* orcid.org/0000-0001-6126-7102; Phone: +92-313-9712930; Email: mohib@bzu.edu.pk, mohibusb@gmail.com; Fax: +92-61-9210071

Suvash Chandra Ojha − *Department of Infectious Diseases, the Affiliated Hospital of Southwest Medical University, Luzhou 646000, China*; Phone: +86 158 8238 2103; Email: suvash_ojha@swmu.edu.cn

Authors

Iqra Ahmad − *Department of Biochemistry, Bahauddin Zakariya University, Multan 66000, Pakistan*

Hira Khalid − *Department of Biochemistry, Bahauddin Zakariya University, Multan 66000, Pakistan*

Asia Perveen − *Department of Biochemistry, Bahauddin Zakariya University, Multan 66000, Pakistan*

Muhammad Shehroz − *Department of Bioinformatics, Kohsar University Murree, Murree 47150, Pakistan*

Umar Nishan − *Department of Chemistry, Kohat University of Science & Technology, Kohat 26000, Pakistan;* orcid.org/0000-0002-0106-3068

Faiz Ur Rahman − *Department of Zoology, University of Shangla, Shangla 19100 Khyber Pakhtunkhwa, Pakistan*

Sheheryar − *Department of Animal Science, Federal University of Ceara, Fortaleza 60020-181, Brazil*

Arlindo Alencar Moura − *Department of Animal Science, Federal University of Ceara, Fortaleza 60020-181, Brazil;* orcid.org/0000-0002-8271-5733

Riaz Ullah − *Department of Pharmacognosy, College of Pharmacy, King Saud University, Riyadh 11451, Saudi Arabia;* orcid.org/0000-0002-2860-467X

Essam A. Ali − *Department of Pharmaceutical Chemistry, College of Pharmacy, King Saud University, Riyadh 11451, Saudi Arabia*

Complete contact information is available at: https://pubs.acs.org/10.1021/acsomega.3c10351

Author Contributions

Resources, conceptualization, supervision, and review & editing: M.S. Formal analysis, investigation, and writing—original draft: I.A., A.P., M.S., U.N., F.U.R., and S. Visualization and review & editing: A.A.M., R.U., U.N., E.A.A., and S.C.O. Funding acquisition: E.A.A. and S.C.O. All authors have read and agreed to the published version of the manuscript. I.A. and H.K. contributed equally to this work.

Funding

This research work was supported by the Researchers Supporting Project Number (RSP2024R45) King Saud University, Riyadh, Saudi Arabia. We also received support from the Doctoral Research Fund awarded to SCO.

Notes

The authors declare no competing financial interest.

■ ACKNOWLEDGMENTS

Authors wish to thank Researchers Supporting Project Number (RSP2024R45) at King Saud University, Riyadh, Saudi Arabia, for financial support. We also thank the Department of Biochemistry, Bahauddin Zakariya University, Multan, Pakistan, for providing the necessary infrastructure to perform this research.

■ REFERENCES

(1) Zagorska, A.; Partyka, A.; Bucki, A.; Gawalskax, A.; Czopek, A.; Pawlowski, M. Phosphodiesterase 10 Inhibitors - Novel Perspectives for Psychiatric and Neurodegenerative Drug Discovery. *Curr. Med. Chem.* **2018**, *25*, 3455−3481.

(2) Siuciak, J. A.; Strick, C. A. Treating neuropsychiatric disorders with PDE10A inhibitors. *Drug Discov. Today Ther. Strat.* **2006**, *3*, 527−532.

(3) Rivera, A.; et al. *Phosphodiesterase 10A (PDE10A): Regulator of Dopamine Agonist-Induced Gene Expression in the Striatum*, 2022.

(4) Geerts, H.; Spiros, A.; Roberts, P. Phosphodiesterase 10 inhibitors in clinical development for CNS disorders. *Expert Rev. Neurother.* **2017**, *17*, 553−560.

(5) Garcia, A. M.; Redondo, M.; Martinez, A.; Gil, C. Phosphodiesterase 10 Inhibitors: New Disease Modifying Drugs for Parkinson's Disease? *Curr. Med. Chem.* **2014**, *21*, 1171−1187.

(6) Ngima Nthenge-Ngumbau, D.; Mohanakumar, K. P. Can. Cyclic Nucleotide Phosphodiesterase Inhibitors Be Drugs for Parkinson's Disease? *Mol. Neurobiol.* **2018**, *55*, 822.

(7) Fox, S. H.; Katzenschlager, R.; Lim, S.; Barton, B.; de Bie, R. M. A.; Seppi, K.; Coelho, M.; Sampaio, C. International Parkinson and movement disorder society evidence-based medicine review: Update on treatments for the motor symptoms of Parkinson's disease. *Mov. Disord.* **2018**, *33*, 1248−1266.

(8) Suzuki, K.; Kimura, H. TAK-063, a novel PDE10A inhibitor with balanced activation of direct and indirect pathways, provides a unique opportunity for the treatment of schizophrenia. *CNS Neurosci. Ther.* **2018**, *24*, 604−614.

(9) Wilson, J. M.; Ogden, A. M. L.; Loomis, S.; Gilmour, G.; Baucum, A. J.; Belecky-Adams, T. L.; Merchant, K. M. Phosphodiesterase 10A inhibitor, MP-10 (PF-2545920), produces greater induction of c-Fos in dopamine D2 neurons than in D1 neurons in the neostriatum. *Neuropharmacology* **2015**, *99*, 379−386.

(10) Czopek, A.; Partyka, A.; Bucki, A.; Pawłowski, M.; Kołaczkowski, M.; Siwek, A.; Głuch-Lutwin, M.; Koczurkiewicz, P.;

Pękala, E.; Jaromin, A.; et al. Impact of N-Alkylamino Substituents on Serotonin Receptor (5-HTR) Affinity and Phosphodiesterase 10A (PDE10A) Inhibition of Isoindole-1,3-dione Derivatives. *Molecules* **2020**, *25*, 3868.
(11) Siuciak, J.; Chapin, D.; Harms, J.. L. L.- & 2006, U *Inhibition of the Striatum-Enriched Phosphodiesterase PDE10A: A Novel Approach to the Treatment of Psychosis*; Elsevier, 2006.
(12) Grauer, S. M.; Pulito, V. L.; Navarra, R. L.; Kelly, M. P.; Kelley, C.; Graf, R.; Langen, B.; Logue, S.; Brennan, J.; Jiang, L.; et al. Phosphodiesterase 10A inhibitor activity in preclinical models of the positive, cognitive, and negative symptoms of schizophrenia. *J. Pharmacol. Exp. Ther.* **2009**, *331*, 574−590.
(13) Bhardwaj, V. K.; Purohit, R. Computer simulation to identify selective inhibitor for human phosphodiesterase10A. *J. Mol. Liq.* **2021**, *328*, 115419.
(14) Chappie, T. A.; Humphrey, J. M.; Allen, M. P.; Estep, K. G.; Fox, C. B.; Lebel, L. A.; Liras, S.; Marr, E. S.; Menniti, F. S.; Pandit, J.; et al. Discovery of a Series of 6,7-Dimethoxy-4-pyrrolidylquinazoline PDE10A Inhibitors†. *J. Med. Chem.* **2006**, *50*, 182−185.
(15) Kehler, J.; Ritzen, A.; Langgård, M.; Petersen, S. L.; Farah, M. M.; Bundgaard, C.; Christoffersen, C. T.; Nielsen, J.; Kilburn, J. P. Triazoloquinazolines as a novel class of phosphodiesterase 10A (PDE10A) inhibitors. *Bioorg. Med. Chem. Lett.* **2011**, *21*, 3738−3742.
(16) Yang, S.-W.; et al. Discovery of orally active pyrazoloquinolines as potent PDE10 inhibitors for the management of schizophrenia. *Bioorg. Med. Chem. Lett.* **2012**, *22*, 235−239.
(17) Ho, G. D.; Michael Seganish, W.; Bercovici, A.; Tulshian, D.; Greenlee, W. J.; Van Rijn, R.; Hruza, A.; Xiao, L.; Rindgen, D.; Mullins, D.; et al. The SAR development of dihydroimidazoisoquinoline derivatives as phosphodiesterase 10A inhibitors for the treatment of schizophrenia. *Bioorg. Med. Chem. Lett.* **2012**, *22*, 2585−2589.
(18) Ho, G. D.; Michael Seganish, W.; Bercovici, A.; Tulshian, D.; Greenlee, W. J.; Van Rijn, R.; Hruza, A.; Xiao, L.; Rindgen, D.; Mullins, D.; et al. The SAR development of dihydroimidazoisoquinoline derivatives as phosphodiesterase 10A inhibitors for the treatment of schizophrenia. *Bioorg. Med. Chem. Lett.* **2012**, *22*, 2585−2589.
(19) Leblond, B.; et al. Substituted 6,7-dialkoxy-3-isoquinoline derivatives as inhibitors of phosphodiesterase 10 (PDE10A). WO 2014071044 A1, 2014.
(20) AbbVie Deutschland GmbH & Co KG. Inhibitors of phosphodiesterase type 10A. EP 2776418 B1, 2017.
(21) Al-Nema, M.; Gaurav, A.; Lee, V. S.; Gunasekaran, B.; Lee, M. T.; Okechukwu, P. Identification of dual inhibitor of phosphodiesterase 1B/10A using structure-based drug design approach. *J. Mol. Liq.* **2021**, *342*, 117485.
(22) Abdelli, I.; Hassani, F.; Brikci, S. B.; Ghalem, S. In silico study the inhibition of angiotensin converting enzyme 2 receptor of COVID-19 by Ammoides verticillata components harvested from Western Algeria. *J. Biomol. Struct. Dyn.* **2021**, *39*, 3263−3276.
(23) Shah, M.; Khan, F.; Ahmad, I.; Deng, C. L.; Perveen, A.; Iqbal, A.; Nishan, U.; Zaman, A.; Ullah, R.; Ali, E. A.; et al. Computer-aided identification of Mycobacterium tuberculosis resuscitation-promoting factor B (RpfB) inhibitors from Gymnema sylvestre natural products. *Front. Pharmacol* **2023**, *14*, 1325227.
(24) Shah, M.; Bashir, S.; Jaan, S.; Nawaz, H.; Nishan, U.; Abbasi, S. W.; Jamal, S. B.; Khan, A.; Afridi, S. G.; Iqbal, A. Computational Analysis of Plant-Derived Terpenes as α -glucosidase Inhibitors for the Discovery of Therapeutic Agents against Type 2 Diabetes Mellitus. *South Afr. J. Bot.* **2021**, *143*, 462−473.
(25) Shah, M.; Yamin, R.; Ahmad, I.; Wu, G.; Jahangir, Z.; Shamim, A.; Nawaz, H.; Nishan, U.; Ullah, R.; Ali, E. A.; et al. In-silico evaluation of natural alkaloids against the main protease and spike glycoprotein as potential therapeutic agents for SARS-CoV-2. *PLoS One* **2024**, *19*, No. e0294769.
(26) Katuwal, S.; Upadhyaya, S. R.; Marahatha, R.; Shrestha, A.; Regmi, B. P.; Khadayat, K.; Basnet, S.; Basnyat, R. C.; Parajuli, N. In Silico Study of Coumarins: Wedelolactone as a Potential Inhibitor of the Spike Protein of the SARS-CoV-2 Variants. *J. Trop. Med.* **2023**, *2023*, 1−19.
(27) Naz, S.; Farooq, U.; Khan, S.; Sarwar, R.; Mabkhot, Y. N.; Saeed, M.; Alsayari, A.; Muhsinah, A. B.; Ul-Haq, Z. Pharmacophore model-based virtual screening, docking, biological evaluation and molecular dynamics simulations for inhibitors discovery against α -tryptophan synthase from Mycobacterium tuberculosis. *J. Biomol. Struct. Dyn.* **2021**, *39*, 610−620.
(28) Daina, A.; Michielin, O.; Zoete, V. SwissADME: A free web tool to evaluate pharmacokinetics, drug-likeness and medicinal chemistry friendliness of small molecules. *Sci. Rep.* **2017**, *7*, 42717.
(29) Bowers, K. J. et al. Scalable Algorithms for Molecular Dynamics Simulations on Commodity Clusters. *ACM/IEEE SC 2006 Conference (SC'06) 43*; IEEE, 2006.
(30) Hildebrand, P. W.; Rose, A. S.; Tiemann, J. K. S. Bringing Molecular Dynamics Simulation Data into View. *Trends Biochem. Sci.* **2019**, *44*, 902−913.
(31) Madhavi Sastry, G.; Adzhigirey, M.; Day, T.; Annabhimoju, R.; Sherman, W. Protein and ligand preparation: parameters, protocols, and influence on virtual screening enrichments. *J. Comput. Aided Mol. Des* **2013**, *27*, 221−234.
(32) Kumar, V.; Saha, A.; Roy, K. Multi-target QSAR modeling for the identification of novel inhibitors against Alzheimer's disease. *Chemom. Intell. Lab. Syst.* **2023**, *233*, 104734.
(33) Geneste, H.; Drescher, K.; Jakob, C.; Laplanche, L.; Ochse, M.; Torrent, M. Novel, potent, selective, and brain penetrant phosphodiesterase 10A inhibitors. *Bioorg. Med. Chem. Lett.* **2019**, *29*, 406−412.
(34) Soon, C. W.; Gautam, V. *New Dual PDE1B and PDE10A Inhibitors Identified via Ligand-Based Pharmacophore Modelling and Virtual Screening*, 2023.
(35) Bhardwaj, V. K.; Purohit, R. Computer simulation to identify selective inhibitor for human phosphodiesterase10A. *J. Mol. Liq.* **2021**, *328*, 115419.
(36) Parcha, P. K.; Sarvagalla, S.; Ashok, C.; Sudharshan, S. J.; Dyavaiah, M.; Coumar, M. S.; Rajasekaran, B. Repositioning antispasmodic drug Papaverine for the treatment of chronic myeloid leukemia. *Pharmacol. Rep.* **2021**, *73*, 615−628.
(37) Pu, X.; Ma, D. Facile Entry to Substituted Decahydroquinoline Alkaloids. Total Synthesis of Lepadins A−E and H. *J. Org. Chem.* **2006**, *71*, 6562−6572.
(38) Casertano, M.; Genovese, M.; Paoli, P.; Santi, A.; Aiello, A.; Menna, M.; Imperatore, C. Insights into Cytotoxic Behavior of Lepadins and Structure Elucidation of the New Alkaloid Lepadin L from the Mediterranean Ascidian Clavelina lepadiformis. *Mar. Drugs* **2022**, *20*, 65.
(39) Shen, L.; Ye, Y.; Wang, X.; Zhu, H.; Xu, C.; Song, Y.; Li, H.; Tan, R. Structure and total synthesis of aspernigerin: A novel cytotoxic endophyte metabolite. *Chem.—Eur. J.* **2006**, *12*, 4393−4396.
(40) Wu, H.; Lu, X.; Xu, J.; Zhang, X.; Xu, H.; Li, Z.; Hou, C.; Yang, X.; Ling, Y. Design, Synthesis, and Fungicidal Activity against Rice Sheath Blight of Novel N-Acyl-1,2,3,4-tetrahydroquinoline Derivatives. *J. Agric. Food Chem.* **2023**, *71*, 11026−11034.
(41) Dekker, K. A.; Inagaki, T.; Gootz, T. D.; Huang, L. H.; Kojima, Y.; Kohlbrenner, W. E.; Matsunaga, Y.; Mcguirk, P. R.; Nomura, E.; Sakakibara, T.; et al. New quinolone compounds from Pseudonocardia sp. with selective and potent anti-Helicobacter pylori activity: Taxonomy of producing strain, fermentation, isolation, structural elucidation and biological activities. *J. Antibiot.* **1998**, *51*, 145−152.
(42) Gonzalo, M:nez-P.; Ricardo, G.-A.; Maricruz, A.-R.; Alan, C.-C. In silico screening of drug Bank data base to PDE10: A drug repurposing approach. *GSC Biol. Pharm. Sci.* **2023**, *24*, 010−021.
(43) Huang, J.; Hu, B.; Xu, Z.; Ye, Y.; Wang, H.; Wang, S.; Liu, Z.; Wang, J. Selectivity mechanism of phosphodiesterase isoform inhibitor through in silico investigations. *J. Mol. Model.* **2022**, *28*, 9.
(44) Bultel-Poncé, V.; Berge, J.-P.; Debitus, C.; Nicolas, J.-L.; Le Guyot, M. *Metabolites from the Sponge-Associated Bacterium Pseudomonas Species*; Springer, 1999.
(45) Adams, M.; Wube, A.; Bucar, F.; Bauer, R.; Kunert, O.; Haslinger, E. Quinolone alkaloids from : a potent new group of

https://doi.org/10.1021/acsomega.3c10351
ACS Omega 2024, 9, 16262−16278

antimycobacterial compounds. *Int. J. Antimicrob. Agents* **2005**, *26*, 262−264.
(46) Chen, I. S.; Wu, S. J.; Tsai, I. L.; Wu, T. S.; Pezzuto, J. M.; Lu, M. C.; Chai, H.; Suh, N.; Teng, C. M. Chemical and bioactive constituents from Zanthoxylum simulans. *J. Nat. Prod.* **1994**, *57*, 1206−1211.
(47) Du, K.; Ma, W.; Yang, C.; Zhou, Z.; Hu, S.; Tian, Y.; Zhang, H.; Ma, Y.; Jiang, X.; Zhu, H.; et al. Design, synthesis, and cytotoxic activities of isaindigotone derivatives as potential anti-gastric cancer agents. *J. Enzyme Inhib. Med. Chem.* **2022**, *37*, 1212−1226.
(48) Molina, P.; Tárraga, A.; Gonzalez-Tejero, A.; Rioja, I.; Ubeda, A.; Terencio, M. C.; Alcaraz, M. J. Inhibition of Leukocyte Functions by the Alkaloid Isaindigotone from Isatis indigotica and Some New Synthetic Derivatives. *ACS Publications* **2001**, *64*, 1297−1300.
(49) Ji, X.; Nielsen, A. L.; Heinis, C. Cyclic Peptides for Drug Development. *Angew. Chem., Int. Ed.* **2024**, *63*, No. e202308251.
(50) Matada, B. S.; Pattanashettar, R.; Yernale, N. G. A comprehensive review on the biological interest of quinoline and its derivatives. *Bioorg. Med. Chem.* **2021**, *32*, 115973.
(51) Pajouhesh, H.; Lenz, G. R. Medicinal chemical properties of successful central nervous system drugs. *NeuroRx* **2005**, *2*, 541−553.
(52) Rasgania, J.; Gavadia, R.; Jakhar, K. Facile synthesis, pharmacological and In silico analysis of succinimide derivatives: An approach towards drug discovery. *J. Mol. Struct.* **2023**, *1274*, 134424.
(53) Bagchi, S.; Chhibber, T.; Lahooti, B.; Verma, A.; Borse, V.; Jayant, R. D. In-vitro blood-brain barrier models for drug screening and permeation studies: An overview. *Drug Des., Dev. Ther.* **2019**, *13*, 3591−3605.
(54) Ota, T.; Kamada, Y.; Hayashida, M.; Iwao-Koizumi, K.; Murata, S.; Kinoshita, K. Combination analysis in genetic polymorphisms of drug-metabolizing enzymes CYP1A2, CYP2C9, CYP2C19, CYP2D6 and CYP3A5 in the Japanese population. *Int. J. Med. Sci.* **2015**, *12*, 78−82.
(55) Pantaleão, S. Q.; Fernandes, P. O.; Gonçalves, J. E.; Maltarollo, V. G.; Honorio, K. M. Recent Advances in the Prediction of Pharmacokinetics Properties in Drug Design Studies: A Review. *ChemMedChem* **2022**, *17*, No. e202100542.
(56) Kadri, A.; Aouadi, K. In vitro antimicrobial and α-glucosidase inhibitory potential of enantiopure cycloalkylglycine derivatives: Insights into their in silico pharmacokinetic, druglikeness, and medicinal chemistry properties. *J. Appl. Pharm. Sci.* **2020**, *10*, 107−115.
(57) White, P. C. Alterations of Cortisol Metabolism in Human Disorders. *Horm Res. Paediatr* **2018**, *89*, 320−330.
(58) Matthews, L. G.; Puryear, C. B.; Correia, S. S.; Srinivasan, S.; Belfort, G. M.; Pan, M.; Kuo, S. T-type calcium channels as therapeutic targets in essential tremor and Parkinson's disease. *Ann. Clin. Transl. Neurol.* **2023**, *10*, 462−483.
(59) Li, Y.; Ji, G.; Lian, M.; Liu, X.; Xu, Y.; Gui, Y. Effect of PLA2G6 and SMPD1 Variants on the Lipid Metabolism in the Cerebrospinal Fluid of Patients with Parkinson's Disease: A Non-targeted Lipidomics Study. *Neurol. Ther.* **2023**, *12*, 2021−2040.
(60) Barrero, F. J.; Ampuero, I.; Morales, B.; Vives, F.; de Dios Luna del Castillo, J.; Hoenicka, J.; García Yébenes, J. Depression in Parkinson's disease is related to a genetic polymorphism of the cannabinoid receptor gene (CNR1). *Pharmacogenomics J.* **2005**, *5*, 135−141.
(61) Vidoni, C.; Follo, C.; Savino, M.; Melone, M. A. B.; Isidoro, C. The Role of Cathepsin D in the Pathogenesis of Human Neurodegenerative Disorders. *Med. Res. Rev.* **2016**, *36*, 845−870.
(62) Politis, M.; Niccolini, F. Serotonin in Parkinson's disease. *Behav. Brain Res.* **2015**, *277*, 136−145.
(63) Amalric, M. Targeting metabotropic glutamate receptors (mGluRs) in Parkinson's disease. *Curr. Opin. Pharmacol.* **2015**, *20*, 29−34.
(64) Li, K.; Wang, M.; Huang, Z. H.; Wang, M.; Sun, W. Y.; Kurihara, H.; Huang, R. T.; Wang, R.; Huang, F.; Liang, L.; et al. ALOX5 inhibition protects against dopaminergic neurons undergoing ferroptosis. *Pharmacol. Res.* **2023**, *193*, 106779.
(65) Shah, M.; Jaan, S.; Shehroz, M.; Sarfraz, A.; Asad, K.; Wara, T. U.; Zaman, A.; Ullah, R.; Ali, E. A.; Nishan, U.; et al. Deciphering the Immunogenicity of Monkeypox Proteins for Designing the Potential mRNA Vaccine. *ACS Omega* **2023**, *8*, 43341−43355.

https://doi.org/10.1021/acsomega.3c10351
ACS Omega 2024, 9, 16262−16278